Final Scientific Report for DOE Award No. DE-FG02-06ER64201

Project Title: **Improving the Representation of Ice Sedimentation Rates in Global Climate Models**

Award recipient: Desert Research Institute, Division of Atmospheric Sciences, 2215 Raggio Parkway, Reno, Nevada 89512-1095

Principle Investigator: Dr. David L. Mitchell

Graduate student funded through this project: Dr. Subhashree Mishra

Project duration: 1 April 2009 – 31 March 2013

Executive Summary:

It is well known that cirrus clouds play a major role in regulating the earth's climate, but the details of how this works are just beginning to be understood. This project targeted the main property of cirrus clouds that influence climate processes; the ice fall speed. That is, this project improves the representation of the mass-weighted ice particle fall velocity, V_m, in climate models, used to predict future climate on global and regional scales.

Prior to 2007, the dominant sizes of ice particles in cirrus clouds were poorly understood, making it virtually impossible to predict how cirrus clouds interact with sunlight and thermal radiation. Due to several studies investigating the performance of optical probes used to measure the ice particle size distribution (PSD), as well as the remote sensing results from our last ARM project, it is now well established that the anomalously high concentrations of small ice crystals often reported prior to 2007 were measurement artifacts. Advances in the design and data processing of optical probes have greatly reduced these ice artifacts that resulted from the shattering of ice particles on the probe tips and/or inlet tube, and PSD measurements from one of these improved probes (the 2-dimensional Stereo or 2D-S probe) are utilized in this project to parameterize V_m for climate models.

Our original plan in the proposal was to parameterize the ice PSD (in terms of temperature and ice water content) and ice particle mass and projected area (in terms of mass- and area-dimensional power laws or m-D/A-D expressions) since these are the microphysical properties that determine V_m, and then proceed to calculate V_m from these parameterized properties. But the 2D-S probe directly measures ice particle projected area and indirectly estimates ice particle mass for each size bin. It soon became apparent that the original plan would introduce more uncertainty in the V_m calculations than simply using the 2D-S measurements to directly calculate V_m. By calculating V_m directly from the measured PSD, ice particle projected area and estimated mass, more accurate estimates of V_m are

obtained. These V_m values were then parameterized for climate models by relating them to (1) sampling temperature and ice water content (IWC) and (2) the effective diameter (D_e) of the ice PSD. Parameterization (1) is appropriate for climate models having single-moment microphysical schemes whereas (2) is appropriate for double-moment microphysical schemes and yields more accurate V_m estimates. These parameterizations were developed for tropical cirrus clouds, Arctic cirrus, mid-latitude synoptic cirrus and mid-latitude anvil cirrus clouds based on field campaigns in these regions.

An important but unexpected result of this research was the discovery of microphysical evidence indicating the mechanisms by which ice crystals are produced in cirrus clouds. This evidence, derived from PSD measurements, indicates that homogeneous freezing ice nucleation dominates in mid-latitude synoptic cirrus clouds, whereas heterogeneous ice nucleation processes dominate in mid-latitude anvil cirrus.

Based on these findings, D_e was parameterized in terms of temperature (T) for conditions dominated by (1) homo- and (2) heterogeneous ice nucleation. From this, an experiment was designed for global climate models (GCMs). The net radiative forcing from cirrus clouds may be affected by the means ice is produced (homo- or heterogeneously), and this net forcing contributes to climate sensitivity (i.e. the change in mean global surface temperature resulting from a doubling of CO_2). The objective of this GCM experiment was to determine how a change in ice nucleation mode affects the predicted global radiation balance. In the first simulation (Run 1), the D_e-T relationship for homogeneous nucleation is used at all latitudes, while in the second simulation (Run 2), the D_e-T relationship for heterogeneous nucleation is used at all latitudes. For both runs, V_m is calculated from D_e. Two GCMs were used; the Community Atmosphere Model version 5 (CAM5) and a European GCM known as ECHAM5 (thanks to our European colleagues who collaborated with us). Similar results were obtained from both GCMs in the Northern Hemisphere mid-latitudes, with a net cooling of ~ 1.0 W m^{-2} due to heterogeneous nucleation, relative to Run 1. The mean global net cooling was 2.4 W m^{-2} for the ECHAM5 GCM while CAM5 produced a mean global net cooling of about 0.8 W m^{-2}. This dependence of the radiation balance on nucleation mode is substantial when one considers the direct radiative forcing from a CO_2 doubling is 4 W m^{-2}. The differences between GCMs in mean global net cooling estimates may demonstrate a need for improving the representation of cirrus clouds in GCMs, including the coupling between microphysical and radiative properties.

Unfortunately, after completing this GCM experiment, we learned from the company that provided the 2D-S microphysical data that the data was corrupted due to a computer program coding problem. Therefore the microphysical data had to be reprocessed and reanalyzed, and the GCM experiments were redone under our current ASR project but using an improved experimental design.

1. Comparison of original project goals with actual accomplishments

The objectives of this project as stated in the original proposal were as follows:

1. Improve or develop cirrus PSD characterizations for the mid-latitudes (synoptic cirrus), the tropics (anvil cirrus) and the Arctic, for use in regional and global climate models.

2. Develop ice particle mass- and projected area-dimensional expressions representative of maritime anvil cirrus, in situ or synoptic cirrus, and Arctic cirrus.

3. Implement the above PSD characterizations and mass/area expressions into the treatment of ice fall speeds in the Community Atmosphere Model version 4 (CAM4). Compare this modified CAM4 with standard CAM4 in simulations ranging from very short to long (~ 20 to 80 year) duration. The short runs examine the altered physical processes while the long runs integrate feedback effects. If deficiencies are revealed in standard CAM4 treatments of cirrus, work with the CAM Atmospheric Model Working Group (AMWG) to resolve these deficiencies.

4. Provide optical properties for ISDAC mixed phase clouds to Paul Lawson at SPEC, Inc.

a. Objectives 1 and 2

Progress was made in parameterizing cirrus PSDs as a function of temperature and IWC for Arctic and anvil cirrus clouds until it was recognized that this was not the best way to parameterize the mass-weighted ice fall speeds, as discussed in the Executive Summary. The same is true for objective 2; power law expressions (derived from observations) that estimate ice particle mass m and projected area A from ice particle maximum dimension D yield m and A values that are less accurate than those directly measured from the 2D-S probe. The 2D-S probe measures A down to 10 μm and estimates m from A using an m-A power law relationship (Baker and Lawson 2006) developed from field observations (Mitchell et al. 1990). Projected area is a better predictor of m than is D (Baker and Lawson 2006). By integrating m over the PSD, an IWC is calculated, and these IWCs compare favorably (generally within a factor of 2) with coincident co-located direct measurements of IWC by the Counterflow Virtual Impactor (CVI) probe (Lawson et al. 2010). For these reasons we used m derived from 2D-S probe measurements of A, and used A, m and the measured PSD to calculate V_m. Subsequently, during our current ASR project, we have verified the Baker-Lawson m-A power law relationship in a variety of ways, including comparisons with other studies.

In retrospect, it was fortunate that we did not follow our original plan to develop m-D and A-D power law expressions based on 2D-S measurements of D, A and m. This is because the 2D-S probe data turned out to be corrupted due to a computer program coding error that was discovered by our

data provider in December of 2012. Once this problem was corrected and the 2D-S data reprocessed, our final method for calculating V_m made the reanalysis process relatively simple and time-efficient. Now using corrected 2D-S data, our current ASR project has determined m-D and A-D expressions as a function of temperature and cirrus cloud type (e.g. anvil vs. synoptic) in order to improve cloud property retrievals from ground- and satellite-based remote sensing platforms.

b. Parameterization of V_m

The central goal of this project was to improve the parameterization of V_m in climate models. As mentioned above, this was done through direct or semi-direct measurements of ice particle size, mass and projected area, along with the ice PSD, using the 2D-S probe. For every PSD measurement V_m was calculated, resulting in 518 calculations of V_m for Arctic, tropical, mid-latitude synoptic and mid-latitude anvil cirrus clouds. For each cloud type excepting Arctic cirrus, V_m was related to temperature and IWC via multiple-regression analysis since this minimized the variance, with r^2 ranging from 0.73 to 0.85, depending on cloud type. For Arctic cirrus, there was no correlation between V_m and IWC, and only a weak correlation between V_m and temperature ($r^2 = 0.25$). These correlations relating V_m to temperature and IWC (or T alone for Arctic cirrus) find value in climate models having single-moment ice cloud microphysics (i.e. only the ice mass mixing ratio or IWC is predicted).

For double moment microphysical schemes (both IWC and ice particle number concentration N are predicted), V_m was related to the effective ice particle diameter D_e of the PSD. Note that $D_e = 3/2\ [IWC/(\rho_i A_{PSD})]$ where ρ_i = density of bulk ice and A_{PSD} = PSD projected area. Since V_m is also a function of ice particle m/A, the correlation between V_m and D_e is very strong, with r^2 between 0.91 (Arctic cirrus) and 0.99 (mid-latitude synoptic and anvil cirrus). These results are described in Mitchell et al. (2011a) and Mishra et al. (2013); the latter is under review and constitutes Appendix A of this report.

A common problem in GCMs is that either the ice cloud radiative properties are completely decoupled from the cloud microphysics, or their interaction is compromised (Baran 2012). For example, the D_e used to calculate ice cloud optical properties may come from a D_e-T relationship and not the GCM microphysical treatment. In Section 5 of Mishra et al. (2013), a simple means of coupling the ice cloud microphysics and radiation is suggested, where V_m is predicted from D_e (predicted from a 2-moment microphysical scheme). Cirrus cloud coverage and IWC/ice water path in essence result from a balance between condensate production in the cloud updraft and condensate removal through precipitation or ice fallout (given by $IWC \times V_m$). Since cirrus cloud radiative forcing and cloud feedback depend mostly on cirrus cloud coverage and ice water path, they also depend strongly on V_m. A secondary dependence is on D_e, which asserts its impact on cloud radiative feedback through the cloud optical properties. By predicting V_m from D_e, the factors responsible for cloud radiative forcing and feedback are automatically coupled and self-consistency is achieved, making the GCM more physically accurate.

c. GCM experiments (objective 3)

The main original objectives regarding the GCM modeling work are listed below:

i. Implement the new treatment of V_m in CAM5 in conjunction with D_e calculations that are consistent with observed D_e values.

ii. Compare this modified CAM5 with the standard CAM5 using both short (5 year) and long (> 20 year) simulations. Evaluate these differences in terms of climate sensitivity.

iii. Use the modified CAM5 to evaluate the radiative effect of introducing more efficient heterogeneous ice nuclei into cold cirrus where homogeneous nucleation otherwise dominates.

All three of these objectives were addressed and either fully or partially completed, but not in the manner originally envisioned. This was partly due to the change in methodology as described above in Section 1.a and partly due to the unanticipated finding of microphysical evidence indicating that homogeneous nucleation, which occurs at temperatures less than -38 °C, dominates ice production in mid-latitude synoptic cirrus clouds (Mitchell et al. 2011b). Regarding the latter, 22 cirrus flights from the 6-month duration SPartICus (Small Particles in Cirrus) field campaign were analyzed for synoptic (13 flights) and anvil (9 flights) cirrus clouds as described in Mishra et al. (2013); see Appendix A. By normalizing the ice particle number concentration N by its corresponding IWC, it was found that N/IWC increased rather abruptly near -40°C. The concentration of ice crystals smaller than 100 μm was also much higher for T < -40°C relative to small ice crystal concentrations at warmer temperatures, especially when normalized by the IWC. Similarly, the PSD mean ice particle size abruptly decreased for T < -40°C. And lastly, an abrupt change in ice particle shape (deduced from ice particle area measurements) occurred near -40°C. These first three observations are predicted to occur when homogeneous freezing nucleation dominates, and the last observation might result from a change in nucleation mechanism. Later it turned out that the last (4^{th}) observation was due to a computer program error that affected the initial data processing as noted above, but the other three observations remained valid after the PSD data was corrected. These findings are described in detail in Mitchell et al. (2011b) and are consistent with the hypothesis that homogeneous nucleation dominates in mid-latitude synoptic cirrus clouds. The reason this was not observed until now is likely due to the problem of ice particle shattering, where a swarm of tiny ice artifacts is produced when relatively large ice particles impact the inlet tube or probe tip of the sampling device. With tiny ice artifacts dominating the ice particle population, it would be impossible to observe these attributes of homogeneous freezing nucleation.

These new findings on the dominance of homogeneous nucleation in synoptic cirrus clouds are closely related to objective iii above. Moreover, these field observations can be used to design a GCM experiment to evaluate the maximum potential radiative impact of efficient heterogeneous ice nucleation on synoptic cirrus clouds where homogeneous nucleation would otherwise dominate. The

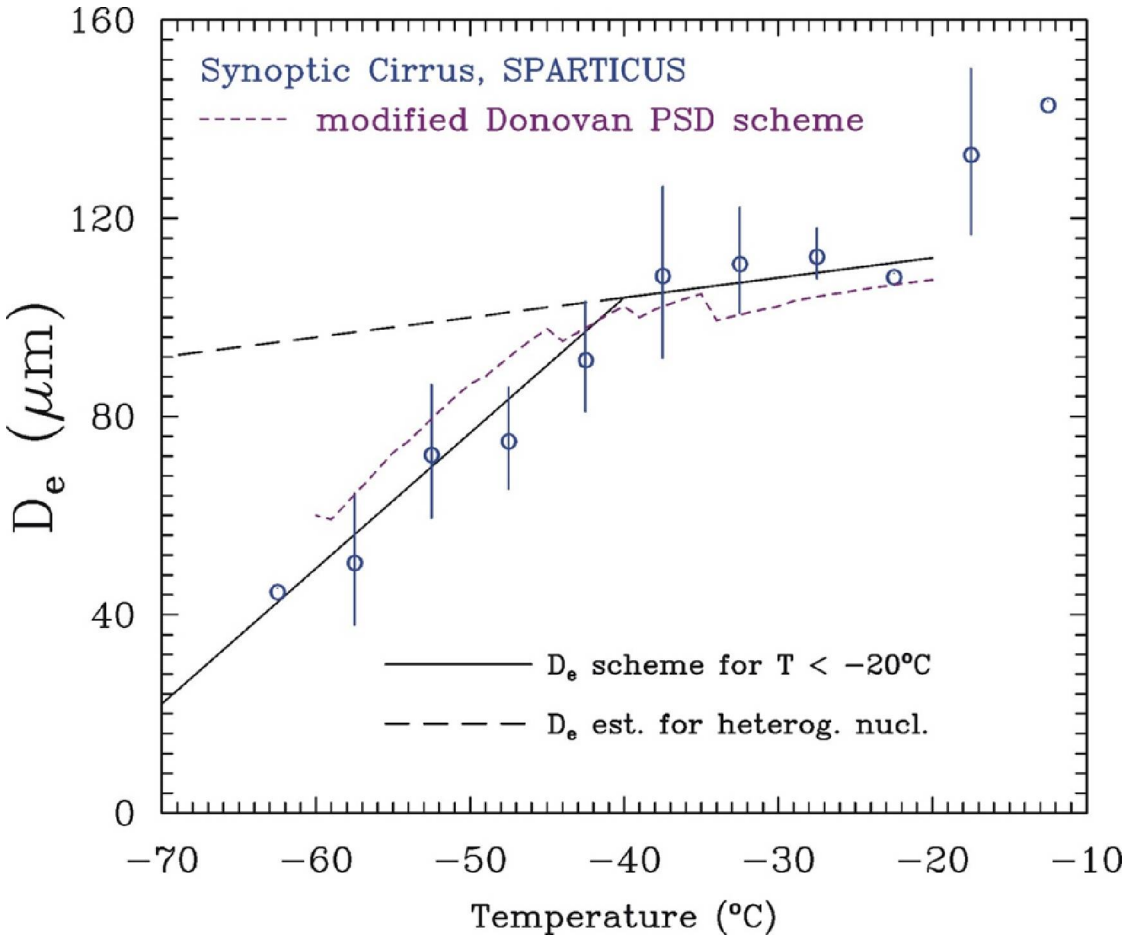

Figure 1. Temperature dependence of D_e in synoptic cirrus clouds observed during the SPartICus Campaign, which served as the basis for a GCM experiment.

essence of this design is shown in Fig. 1, where D_e from synoptic cirrus PSD is related to PSD sampling temperature. Vertical bars are standard deviations for D_e. Linear fits to the data are shown by solid lines for the temperature region dominated by homogeneous nucleation (T < -40°C) and heterogeneous nucleation for -40°C < T < -20°C. The latter was extrapolated to colder temperatures via the dashed line, and together these dashed and solid lines constitute the D_e-T relationship for heterogeneous nucleation (considered an upper limit for D_e resulting from heterogeneous nucleation). The two solid lines represent the synoptic cirrus observations and the D_e-T relationship for homogeneous (T < -40°C) and heterogeneous nucleation. For T > -20°C, D_e is likely to be affected by the aggregation growth process, and the standard GCM microphysics predicts D_e. The purple short-dashed curve is the D_e-T relationship predicted by the Donovan PSD scheme after its predicted concentration of small ice crystals have been corrected as described in Mitchell et al. (2010).

The GCM experiment consisted of three 5-year simulations: a standard simulation using climatological sea surface temperatures (the control run); Run 1 using the homogeneous and heterogeneous D_e-T relationships (solid lines in Fig. 1); and Run 2 using the D_e-T relationship for only

heterogeneous nucleation (dashed and solid lines in Fig. 1). To realistically couple the ice cloud microphysics and radiation modules, and to produce more realistic cirrus cloud radiative forcing as described above in Sec. 1b, V_m was predicted from D_e as described in Mitchell et al. (2011a). These changes were applied to all latitudes. Since the representation of cirrus clouds differs between GCMs, two GCMs were used: (1) the Community Atmosphere Model version 5 (CAM5), and (2) a European GCM known as ECHAM5. The ECHAM5 simulations were made possible through collaborations with Professor Ulrike Lohmann and her Ph.D. student Miriam Kuebbeler at ETH Zurich, Switzerland. The difference in net cloud radiative forcing between Runs 1 and 2 (Run 2 – Run 1) is shown in Fig. 2 as a function of latitude for both GCMs as zonal mean values. Similar patterns of net cloud forcing are apparent between GCM experiments although the magnitude of the forcing differs, with net cooling in the Northern Hemisphere mid-latitudes of about -1 W m^{-2} for CAM5 and about -2 W m^{-2} for ECHAM5. This forcing is considerable when one considers that the direct forcing from a CO_2 doubling is 4 W m^{-2}. The term "negative Twomey effect" has been coined (Kärcher and Lohmann 2003) to describe this cooling effect.

The negative Twomey effect could have been investigated in a more rigorous manner using parameterizations of ice nucleation mechanisms and ice particle growth processes (e.g. vapor deposition and aggregation), but ice nucleation and aggregation rates have relatively high uncertainties. For this reason it makes sense to identify conditions in field experiments dominated by homo- and heterogeneous ice nucleation, and develop GCM experiments based on observations of these conditions as described here.

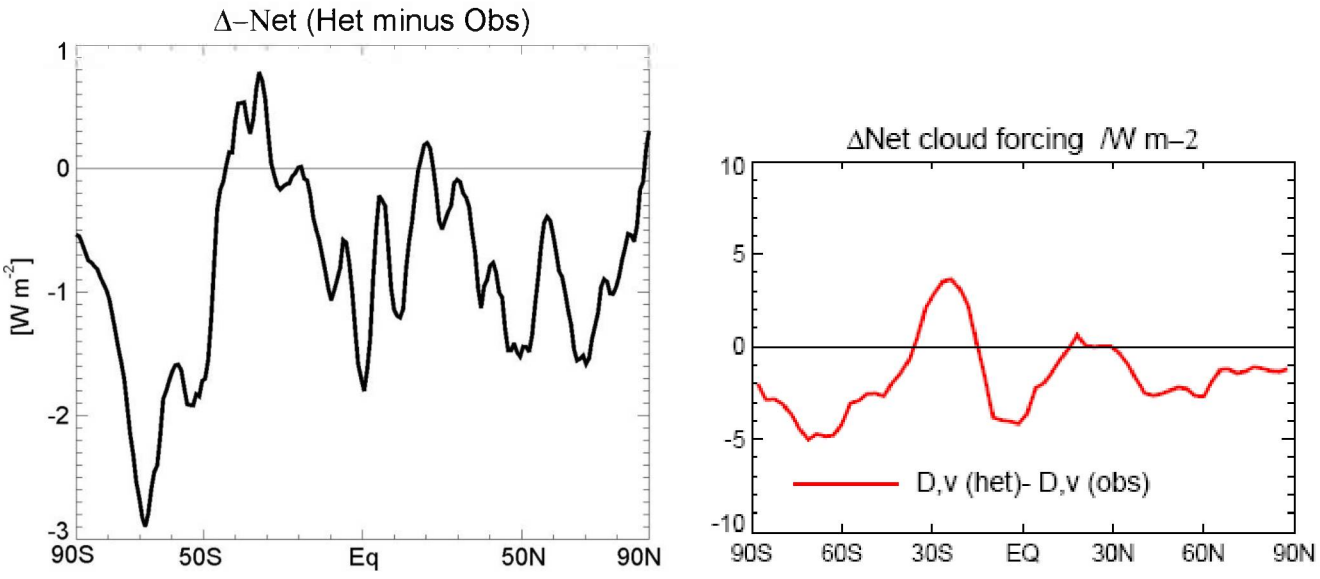

Figure 2. Maximum net radiative cooling expected from changing from homo- to hetero-geneous nucleation in CAM5 (left) and ECHAM5 (right). Note differences in scale (W m^{-2}).

A recent paper in Science (Cziczo et al. 2013) argues that mineral dust is ubiquitous in the atmosphere and that heterogeneous nucleation is the dominant nucleation pathway for the clouds sampled, based on in situ measurements of the composition of the residual particles from sublimated ice crystals. If these findings are universal, then the negative Twomey effect may rarely occur, if ever. The Cziczo et al. study was based on four field campaigns, CRYSTAL-FACE, TC4, CRAVE, and MACPEX. In the first three, anvil cirrus clouds were sampled, while both anvil and synoptic cirrus clouds were sampled during MACPEX. It is not surprising for mineral dust concentrations to be sufficient for heterogeneous nucleation to dominate in anvil cirrus since deep convection advects dust-rich boundary layer air to cirrus levels. Moreover, MACPEX was conducted during March and April, which are the two months of the year when east Asian dust storms are most active (dust from these storms are generally lofted much higher than Saharan dust). It thus appears possible that homogeneous nucleation might dominate in synoptic cirrus during periods where dust concentrations at cirrus levels are much lower. This apparently was the case during the cirrus flights we analyzed from SPartICus, and most of the PSDs we analyzed were obtained during January and February when dust levels are typically ~ 1/3 of Spring levels (Yu et al. 2012). This suggests that heterogeneous nucleation prevailing in synoptic cirrus clouds over North America might be episodic in nature, possibly related to East Asian dust events. This also suggests that the negative Twomey effect may occur episodically with associated changes in cirrus cloud radiative forcing. If dust storms are increasing in frequency, their associated cooling effect could "mask" some of the greenhouse gas warming that would otherwise occur.

In November of 2012, the company that provided us with 2D-S measurements (SPEC, Inc.) discovered that the 2D-S data was corrupted due to a "bug" in the computer code used to process the 2D-S PSD data. This required SPEC, Inc. to reprocess all the data and it required us to conduct another level of data reprocessing with subsequent data reanalysis. It also meant that the two GCM experiments described above had to be redone. These two experiments were redone under our new ASR project, and the experimental design has been improved considerably. The results are not very different than those reported here.

d. Calculating the optical properties of ice clouds and mixed phase clouds (objective 4)

As part of our collaboration with SPEC, Inc., we developed treatments of optical properties for ice clouds and for mixed phase clouds. Both treatments use in situ microphysical measurements as input for these cloud optical property computer programs that we developed for SPEC, Inc. This input consists of the 2D-S size distributions of cloud particle number, projected area and mass, along with the percentages of various ice particle shapes observed. The optical properties are formulated such that they can be calculated directly from these measurements. This approach differs markedly from the more traditional approach that relies on idealized models of ice crystals and calculates optical properties from these models. The ice particle optical property code developed here is based on

Mitchell et al. (1996), Mitchell (2002) and Mitchell et al. (2006), while the cloud droplet optical properties are based on Mitchell (2000). Results from this collaboration are reported in Lawson et al. (2010). Another paper on ISDAC mixed phase clouds, describing their microphysical and radiative properties, is in preparation at SPEC.

2. Departures from planned methodology

The above section describes some of the departures from planned methodology. These departures can be summarized as follows:

1) Instead of calculating V_m from parameterized PSD and m-D/A-D power law expressions, we calculated V_m directly from 2D-S probe measurements of size distributions of ice particle number, projected area and mass. This greatly reduced uncertainties and increased accuracy.
2) Instead of predicting V_m in CAM5 from PSDs and m-D/A-D expressions, V_m was predicted from D_e where the V_m-D_e relationship was based on 2D-S probe observations. Like V_m, D_e was calculated directly from 2D-S measurements of ice particle area and mass. This approach reduced uncertainties and increased accuracy in predicting V_m in CAM5.
3) Long GCM simulations of 20-80 years, designed to estimate climate sensitivity, were not conducted. The original plan was to use a large computer from Pacific Northwest National Laboratories (PNNL) through our collaboration with Dr. Philip Rasch. Dr. Rasch enabled us to use a PNNL computer after months of effort. Just when we were almost ready to actually begin working with the PNNL computer, a cluster computer, purchased during a recent NSF EPSCoR project, became available at DRI. This DRI computer was capable of running 5-year CAM5 simulations in about one week (but using 50% of CPU capacity), making it practical to use for most of our needs. However, the long simulations for climate sensitivity were not practical. Since it was much easier and efficient to use the new DRI computer, we focused on 5-year simulations addressing the negative Twomey effect, which was the 3rd modeling objective. The 2nd modeling objective, comparing modified CAM5 with the standard CAM5, was still done but using shorter 5-year runs.

   Differences in net radiative cloud forcing between standard CAM5 and either Run 1 or 2 were similar to the differences reported above regarding Runs 1 and 2. Since Run 1 was based entirely on observations, differences between Run 1 and the control run should be helpful for developing future improvements in CAM5.

3. Publications

a. Journal Publications

Some of the journal articles listed below resulted from research initiated during our previous ASR project, but these efforts culminated in peer-reviewed publications during this project.

Mishra, S., D.L. Mitchell, and D. DeSlover, 2009: Ground based retrievals of small ice crystals and water phase in Arctic cirrus. AIP Conference Proceedings 1100, *Current Problems in Atmospheric Radiation (IRS 2008)*, Proceedings of the International Radiation Symposium (IRC/IAMAS), Eds. Teruyuki Nakajima and Marcia Akemi Yamasoe, Foz de Iguassu, Brazil, 3-8 August 2008, 482-485.

Mitchell, D.L., and R.P. d'Entremont, 2009: Satellite remote sensing of small ice crystal concentrations in cirrus clouds. AIP Conference Proceedings 1100, *Current Problems in Atmospheric Radiation (IRS 2008)*, Proceedings of the International Radiation Symposium (IRC/IAMAS), Eds. Teruyuki Nakajima and Marcia Akemi Yamasoe, Foz de Iguassu, Brazil, 3-8 August 2008, 185-188.

Mitchell, D.L. and W. Finnegan, 2009: Modification of cirrus clouds to reduce global warming. *Environ. Res. Lett.*, **4**, 045102 (8 pp), doi:10.1088/1748-9326/4/4/045102. Available at: http://iopscience.iop.org/search;jsessionid=0E14B744402F5B493C69A31D0534679A.c1?searchType=fullText&fieldedquery=Modification+of+cirrus+clouds+to+reduce+global+warming&f=titleabs&time=threeyear&issn=1748-9326&submit=Search&navsubmit=Search

Mitchell, D.L., R.P. d'Entremont and R.P. Lawson, 2010: Inferring cirrus size distributions through satellite remote sensing and microphysical databases. *J. Atmos. Sci.*, **67**, 1106-1125.

Mitchell, D.L., R.P. Lawson and B. Baker, 2010: Understanding effective diameter and its application to terrestrial radiation in ice clouds. *Atmos. Chem. Phys. Discuss.*, **10**, 29405-29447, doi:10.5194/acpd-10-29405-2010.

Lawson, R.P., E. Jensen, D.L. Mitchell, B. Baker, Q. Mo and B. Pilson, 2010: Microphysical and Radiative Properties of Tropical Clouds Investigated in TC4 and NAMMA. *J. Geophys. Res.*, **115**, D00J08, doi:10.1029/2009JD013017.

Gettelman, A., X. Liu, S. J. Ghan, H. Morrison, S. Park, A. J. Conley, S. A. Klein, J. Boyle, D. L. Mitchell, and J.-L. F. Li, 2010: Global simulations of ice nucleation and ice supersaturation with an improved cloud scheme in the Community Atmosphere Model, *J. Geophys. Res.*, **115**, D18216, doi:10.1029/2009JD013797.

Mitchell, D. L., R. P. Lawson and B. Baker, 2011: Understanding effective diameter and its application to terrestrial radiation in ice clouds. *Atmos. Chem. Phys.*, **11**, 3417-3429.

Mitchell, D. L., S. Mishra, and R. P. Lawson, 2011: Representing the ice fall speed in climate models: Results from Tropical Composition, Cloud and Climate Coupling (TC4) and the Indirect and Semi-Direct Aerosol Campaign (ISDAC), *J. Geophys. Res.*, **116**, D00T03, doi:10.1029/2010JD015433.

Mitchell, D. L., and R. P. d'Entremont, 2011: Satellite retrieval of the liquid water fraction in tropical clouds between -20° and -38°C. *Atmos. Meas. Tech. Discuss*., **4**, 1-42, doi:10.5194/amtd-4-1-2011.

Mitchell, D. L., and R. P. d'Entremont, 2012: Satellite retrieval of the liquid water fraction in tropical clouds between -20 and -38°C. *Atmos. Meas. Tech*., **5**, 1683–1698, doi:10.5194/amt-5-1683-2012.

Liu, X., Easter, R. C., Ghan, S. J., Zaveri, R., Rasch, P., Shi, X., Lamarque, J.-F., Gettelman, A., Morrison, H., Vitt, F., Conley, A., Park, S., Neale, R., Hannay, C., Ekman, A. M. L., Hess, P., Mahowald, N., Collins, W., Iacono, M. J., Bretherton, C. S., Flanner, M. G., and Mitchell, D., 2012: Toward a minimal representation of aerosols in climate models: description and evaluation in the Community Climate Model CAM5, *Geosci. Model Development*, **5**, 709-739, doi:10.5194/gmd-5-709-2012.

Mishra, S., D. L. Mitchell, D. D. Turner and R. P. Lawson, 2013: Parameterization of ice fall speeds in mid-latitude cirrus: Results from SPartICus. Submitted to J. Geophys. Res. in July, 2013.

b. Book chapters and book reviews

Mitchell, D. L., S. Mishra and R. P. Lawson, 2011: Cirrus clouds and climate engineering: New findings on ice nucleation and theoretical basis. In: *Planet Earth 2011 - Global Warming Challenges and Opportunities for Policy and Practice*, Prof. Elias Carayannis (Ed.), ISBN 978-953-307-733-8, InTech, Available from <http://www.intechopen.com/articles/show/title/cirrus-clouds-and-climate-engineering-new-findings-on-ice-nucleation-and-theoretical-basis>

Mitchell, D. L., 2011: Book review of "Geo-engineering Climate Change: Environmental Necessity or Pandora's Box?", Brian Launder and J. Michael T. Thompson (Eds.), 2010, 332 pp., Cambridge Univ. Press, ISBN 978-0-521-19803-5. *Bull. Amer. Meteorol. Soc*., **92**, 1503-1504.

c. Conference papers

d'Entremont, R.P., and D.L. Mitchell, 2009: A causational argument for the influence of contrail ice particle shape on thermal infrared radiance observations. AMS Annual Meeting, Phoenix, Arizona, January 2009.

Mitchell, D.L., 2009: New understanding of split-window emissions provides insight on small ice crystal concentrations. Hyperspectral Imaging and Sensing of the Environment (HISE), *Technical Digest*, Optical Society of America.

Mitchell, D.L., and R.P. d'Entremont, 2011: Satellite Retrieval of Percent Liquid Water in Tropical Clouds Between -20° and -38°C. Hyperspectral Imaging and Sensing of the Environment (HISE), *Technical Digest*, Optical Society of America.

d. Conference presentations

Mitchell, D.L., S. Mishra and R.P. Lawson, 2011: Modification of cirrus clouds to reduce global warming: New findings. American Geophysical Union Fall Meeting, oral presentation, San Francisco, California, 5-9 December 2011.

Mitchell, D. L., J. Mejia, M. Xiao, P. Rasch, M. Kuebeller: Cirrus cloud climate engineering. International Conference on Clouds and Precipitation (ICCP), oral presentation, Leipzig, Germany, 29 July – 3 August 2012.

e. Invited seminars

Mitchell, D.L., and S. Mishra, 2011: Engineering of cirrus clouds to reduce global warming. International Union of Geophysics and Geodesy (IUGG), IUGG XV General Assembly, "Earth on the edge: Science for a Sustainable Planet", 28 June – 7 July 2011, Melbourne, Australia. Invited by steering committee of Union Session U-06: Geoengineering: What are the Potentials for Climate Intervention, Carbon Scrubbing, and other Approaches to Moderate Climate Change and its Impacts?

Mitchell, D.L., 2012: Manipulating cirrus clouds. IMPLICC Final Symposium: The Atmospheric Science and Economics of Climate Engineering via Aerosol Injections, Max Planck Institute for Chemistry, Mainz, Germany, 14-16 May 2012.

f. Ph.D. dissertation

Mishra, Subhashree, 2011: An investigation of cloud processes relevant to climate sensitivity. University of Nevada, Reno, 153 pp.

4. Collaborations

a. SPEC, Inc.

Our collaboration with SPEC, Inc. supplied us with measurements of ice cloud microphysical properties with assistance from SPEC scientists on data processing. After SPEC discovered that a coding error had corrupted the data, SPEC reprocessed the data using a method that was best suited to

our research needs. On our side, we provided SPEC with computer programs for calculating the optical properties of ice clouds and mixed phase clouds.

b. ETH, Zurich, Switzerland

Near the end of this project an unexpected collaboration developed with Professor Ulrike Lohmann's group at ETH Zurich, Switzerland, who are seeking to understand the impact of homo- vs. heterogeneous nucleation on cirrus cloud radiative forcing. The GCM experiment reported in Sec. 1c demonstrates preliminary progress on this issue. By conducting the experiment using two GCMs, some measure of uncertainty in cirrus cloud radiative forcing due to the negative Twomey effect can be assessed. Through this collaboration we were able to show that the treatment of cirrus clouds in GCMs varies considerably in regards to their contribution to cloud radiative forcing and the predicted magnitude of the negative Twomey effect.

c. Pacific Northwest National Laboratory (PNNL)

Dr. Philip Rasch, Chief Climate Scientist at PNNL, collaborated with us in developing expertise to run the CAM5 GCM. Dr. Rasch was very generous with his limited time and enabled us to conduct the modeling work in this project.

REFERENCES

Baker, B. and R. P. Lawson, 2006: Improvement in determination of ice water content from two-dimensional particle imagery. Part I: Image-to-mass relationships. *J. Appl. Meteor. Climatol.*, **45**, 1282-1290.

Baran, A. J., 2012: From the single-scattering properties of ice crystals to climate prediction: A way forward. *Atmos. Res.*, **112**, 45-69.

Cziczo, D. J., K. D. Froyd, C. Hoose, E. J. Jensen, M. Diao, M. A. Zondlo, J. B. Smith, C. H. Twohy, D. M. Murphy, 2013: Clarifying the Dominant Sources and Mechanisms of Cirrus Cloud Formation. *Science*, **340**, 1320-1324.

Kärcher, B. and U. Lohmann, 2003: A parameterization of cirrus cloud formation: Homogeneous freezing. *J. Geophys. Res.*, **108**, No. D14, 4402, doi:10.1029/2002JD003220.

Lawson, R. P., E. Jensen, D. L. Mitchell, B. Baker, Q. Mo, and B. Pilson, 2010: Microphysical and radiative properties of tropical clouds investigated in TC4 and NAMMA. *J. Geophys. Res.*, **115**, D00J08.

Mishra, S., D. L. Mitchell, D. D. Turner and R. P. Lawson, 2013: Parameterization of ice fall speeds in mid-latitude cirrus: Results from SPartICus. Submitted to J. Geophys. Res. in July, 2013.

Mitchell, D.L., R. Zhang and R.L. Pitter, 1990: Mass-dimensional relationships for ice particles and the influence of riming on snowfall rates. *J. Appl. Meteor.*, **29**, 153-163.

Mitchell, D.L., A. Macke, and Y. Liu, 1996b: Modeling cirrus clouds. Part II: Treatment of radiative properties. *J. Atmos. Sci.*, **53**, 2967-2988.

Mitchell, D.L., 2000: Parameterization of the Mie extinction and absorption coefficients for water clouds. *J. Atmos. Sci.*, **57**, 1311-1326.

Mitchell, D.L., 2002: Effective diameter in radiation transfer: General definition, applications and limitations. *J. Atmos. Sci*, **59**, 2330-2346.

Mitchell, D. L., A. J. Baran, W. P. Arnott and C. Schmitt, 2006: Testing and Comparing the Modified Anomalous Diffraction Approximation. *J. Atmos. Sci.*, **63**, 2948-2962.

Mitchell, D.L., d'Entremont, R. P., & Lawson, R. P., 2010: Inferring cirrus size distributions through satellite remote sensing and microphysical databases. *J. Atmos. Sci.*, **67**, 1106-1125.

Mitchell, D. L., S. Mishra, and R. P. Lawson, 2011(a): Representing the ice fall speed in climate models: Results from Tropical Composition, Cloud and Climate Coupling (TC4) and the Indirect and Semi-Direct Aerosol Campaign (ISDAC), *J. Geophys. Res.*, **116**, D00T03, doi:10.1029/2010JD015433.

Mitchell, D. L., S. Mishra and R. P. Lawson, 2011(b): Cirrus clouds and climate engineering: New findings on ice nucleation and theoretical basis. In: *Planet Earth 2011 - Global Warming Challenges and Opportunities for Policy and Practice*, Prof. Elias Carayannis (Ed.), ISBN 978-953-307-733-8, InTech, Available from <http://www.intechopen.com/articles/show/title/cirrus-clouds-and-climate-engineering-new-findings-on-ice-nucleation-and-theoretical-basis>

Yu, H., L. A. Remer, M. Chin, H. Bian, Q. Tan, T. Yuan and Y. Zhang, 2012: Aerosols from Overseas Rival Domestic Emissions over North America. *Science*, **337**, 566-569.

APPENDIX A

This appendix provides a draft copy of the following paper submitted to Journal of Geophysical Research:

Mishra, S., D. L. Mitchell, D. D. Turner and R. P. Lawson, 2013: Parameterization of ice fall speeds in mid-latitude cirrus: Results from SPartICus. Submitted to J. Geophys. Res. in July, 2013.

This paper, along with Mitchell et al. (2011a) and Mitchell et al. (2011b) cited in Sec. 3a, contains the core findings of this project that relate to the prediction of V_m in climate models and the relative importance of homo- and heterogeneous ice nucleation in mid-latitude synoptic cirrus clouds. Section 3 of Mitchell et al. (2011b) is will soon be revised for journal publication.

Parameterization of Ice Fall Speeds in Mid-Latitude cirrus: Results from SPartICus

Subhashree Mishra[1,2], David L. Mitchell[2], David D. Turner[3], R. P. Lawson[4],

1. Cooperative Institute for Mesoscale Meteorological Studies, Norman, OK

2. Desert Research Institute, Reno, NV

3. NOAA National Severe Storms Lab., Norman, OK

4. SPEC Inc., Boulder, CO

Corresponding Author: Subhashree Mishra, 120 David L. Boren Blvd., Norman, OK, 73072-7303 (subh.mishra@gmail.com)\

Abstract

The climate sensitivity of global climate models (GCMs) can be sensitive to the treatment of the ice particle fall velocity (Sanderson et al. 2008). In this study, the mass weighted ice fall speed (V_m) in mid-latitude cirrus clouds is computed from in-situ measurements of ice particle area and number concentration made by the 2-dimensional Stereo (2D-S) probe during the Small Particles In Cirrus (SPartICus) field campaign. V_m in mid-latitude cirrus is parameterized in terms of cloud temperature (T) and ice water content (IWC), and also by relating V_m to the ice particle size distribution effective diameter (D_e). Although the correlations of V_m and D_e with T were higher than the correlations of V_m and D_e with IWC, it is demonstrated that V_m and D_e are better predicted by using both T and IWC. The parameterization relating V_m to T and IWC is compared with another scheme relating V_m to T and IWC, with the latter based on Millimeter Cloud Radar (MMCR) measurements. Results also show a strong correlation between D_e and V_m owing to their similar mathematical formulations. Estimating V_m from D_e makes V_m a function of IWC and projected area, realistically coupling V_m with both the cloud microphysics and radiative properties.

1. Introduction

While General Circulation Models (GCMs) represent the most complete description of all the interactions between the processes that define the primary cloud feedbacks on climate (Stephens 2005), this description is highly sensitive to the

representation of clouds and their feedbacks. Despite increased computing power, the vast range of temporal and spatial scales associated with cloud processes requires substantial simplifications for representing clouds in current GCMs (Morrison and Gettelman 2008). Such simplification of cloud processes is achieved through the parameterization of many of these processes. Earlier studies have shown that the sensitivity of GCMs is highly dependent on the way clouds are parameterized (Fowler and Randall 1994; Ma et al.1994). Thus, one of the weakest links in the use of GCMs lies in the cloud parameterization imbedded in them (Stephens 2005).

Sanderson et al. (2008) used the Hadley Centre atmospheric model (HadAM3) and performed a linear analysis using a multi-thousand member perturbed physics ensemble to relate climate sensitivity S [defined as the equilibrium response of global-mean surface temperature to a CO_2 doubling] to atmospheric GCM model parameters. Based on their study, the physical processes that accounted for 70% of the variance in the global feedback parameter λ ($\lambda = 1/S$) were due to two leading factors: the entrainment coefficient and the ice fall velocity (V_i). The ice fall-velocity has a strong impact on cloud radiative forcing and climate feedback due to its influence on cirrus cloud lifetime (i.e. coverage), optical thickness (via ice water path) and upper tropospheric water vapor (Mitchell et al. 2008; Mitchell and Finnegan 2009), which is very important for determining climate sensitivity (Sanderson, 2011).

In spite of its importance, V_i in climate models is highly uncertain, due in part to its dependence on the ice particle size distribution (PSD), which has been plagued with measurement uncertainties. Historical measurements of ice crystal concentrations, mass,

and area have been erroneous owing to the presence of large concentrations of small (< 60 μm) ice crystals produced due to the shattering of larger ice crystals on inlets of cloud probes. Recently, data processing techniques used in conjunction with new probes in recent field campaigns appear to have significantly reduced the artifact concentration of small ice particles (Lawson, 2011). The focus of this study is to improve the parameterization of the mass weighted ice fall velocity (V_m) in GCMs by using data from the new and improved 2 Dimensional-Stereo (2D-S) cloud probe. In this regard, ice fall speed parameterizations for mid-latitude cirrus clouds (both anvil and synoptic cirrus) are presented.

Ice sedimentation rates in cirrus are the product of V_m and the corresponding ice water content (IWC). The value of V_m depends upon the median mass dimension of the PSD, the PSD shape such as the degree of bimodality, the ice particle shapes comprising the PSD, and the air temperature and pressure (Mitchell et al., 2011b). Parameterization of V_m is achieved by relating it to temperature (T) and ice water content (IWC). V_m is also related to the effective diameter (D_e). It is shown that the relation of V_m to D_e is better for parameterization purposes than the relation of V_m to (T and IWC). In addition, this paper also compares ice fall speeds obtained by using in-situ aircraft data from the 2D-S probe against fall speeds computed from Doppler radar measurements as presented in Deng and Mace (2006, 2008).

The theory of fall speed formulation used in this paper is presented in section 2. The methodology describing the field campaign, measurements and data analysis

methods is presented in section 3, followed by results in section 4. Summary and conclusions are presented in section 5.

2. Theory

This section provides a brief overview of the physics of free falling solid hydrometeors (ice particles). The net force (F_{net}) experienced by a particle falling through the atmosphere can be expressed as

$$F_{net} = F_g - F_D \quad (1)$$

where F_g is the gravitational force on a particle of mass m (F_g = m g where g = acceleration due to gravity). F_D is the drag force exerted on the particle by the air displaced by the particle. The drag force is a function of the properties of the particle and the medium (air) through which it falls and can be expressed as

$$F_D = \frac{1}{2}\rho_a {v_t}^2 A C_D \quad (2)$$

where ρ_a is the density of air, v_t is the particle's terminal fall speed, A is the area of cross section of the particle projected normal to the flow and C_D is the drag coefficient. The terminal velocity (v_t) of the particle is the maximum speed attained by the particle when $F_D = F_g$ and can be expressed as

$$v_t = \left(\frac{2mg}{\rho_a A C_D}\right)^{1/2}. \qquad (3)$$

Thus the terminal velocity of the particle is dependent on C_D and on two other properties of the particle, namely the mass and the area. The formulation of v_t in equation 3 has dependence on C_D which is difficult to characterize independent of v_t. Hence, a theoretical relationship between the Reynolds number (Re) and the Best or Davies number (X), formulated by Bohm (1989, 1992) is used to calculate v_t as described in Mitchell (1996) since X is independent of the terminal velocity, v_t (Davies 1945). The Reynolds number, a ratio of the inertial to viscous forces, is expressed as

$$Re = \frac{v_t D}{\nu} = \frac{\rho_a v_t D}{\eta} \qquad (4)$$

where D is the maximum dimension of the particle, ν is the kinematic viscosity (note that $\nu = \eta/\rho_a$ and η is dynamic viscosity. As explained in Pruppacher and Klett (1997), the Best number is related to the Reynolds number by the relationship

$$X = C_D\, Re^2 = \frac{2mg\rho_a D^2}{A\eta^2} \quad . \qquad (5)$$

The above equation is part of the theoretical basis used for deriving ice particle fall velocities by Mitchell 1996 (henceforth M96), Mitchell and Heymsfield 2005 (henceforth MH05) and Heymsfield and Westbrook 2010 (henceforth HW10). Combined with a theoretical expression for C_D, this Re–*X* formula can be rearranged to give a continuous analytical function that yields terminal velocities for any ice particle type (Bohm 1989). While Bohm's methods are generalized for all particle types and used idealized shapes or

spheroids to represent ice particles, later papers employed a more realistic criterion (projected area and mass-dimensional power-law expressions) to account for the irregular shapes associated with ice crystals.

2.1. Fall speed formulation of Heymsfield and Westbrook 2010 (HW10)

In this study, the HW10 scheme is used to calculate V_m. The formulation of HW10 was shown to be more accurate for ice particles having aspect ratios far from unity, such as long columns, needles and dendritic ice crystals. The earlier fall speed schemes had errors of up to 80% for small particles (smaller than 100 μm), where the air flow is dominated by viscous forces. Based on comparisons with various laboratory, tank and field experiments, HW10 show that the error in calculation of fall speed using their new scheme is within 30% of experimental data presented in Westbrook 2008.

Based on extensive measurements, HW10 suggested that the fall speeds of ice particles were more sensitive to changes in ice particle aspect ratios than predicted by M96 and MH05. While the observation-derived fallspeeds of ice crystals having aspect ratios near unity agreed well with those predicted by M96, fallspeeds for extreme aspect ratio ice crystals differed considerably. Hence they proposed to use a modified drag coefficient that resulted in a modified Best number formulation. Other modifications included redefining the limiting pressure drag constant (i.e. the potential flow drag coefficient) $C_o = 0.35$ (dimensionless) and the dimensionless boundary layer constant $\delta_o = 8.0$, which are used to calculate Reynolds number (Re) from X. The formulation of fall speed by HW10 is similar to that of M96 but the fall-speed dependence on particle projected area is reduced by redefining the Best number X as

$$X = \frac{\rho_a}{\eta^2}\frac{8mg}{\pi A_r^{0.5}} \qquad (6)$$

where A_r is the ice particle area ratio (actual projected area divided by area of circumscribed circle). These modifications result in significantly more accurate fall speeds for some ice crystals such as thin planar crystals (e.g. stellar dendrites) or long columnar crystals (e.g. long columns and needles), but HW10 differs only slightly from the MH05 scheme when ice crystals have aspect ratios near unity (based on results presented in Fig. 1 in this paper and in Mitchell et al. 2011b). The above formulation of HW10 was rewritten in Mitchell et al. (2011b) to replace area ratio of ice particles with the area projected to the flow since previous investigators have defined the Best number in terms of projected area. Thus, the modified version of the above equation can be written as

$$X = \frac{\rho_a}{\eta^2}\frac{4mgD}{\pi^{0.5}A^{0.5}} \quad . \qquad (7)$$

While the HW10 scheme satisfies the theoretical expectation $C_o\delta_o^2 \approx 24$ (for details refer to equation 10.39, page 370 in Pruppacher and Klett 1997), the value of C_o estimated from laboratory measurements (Bohm 1989; Lamb and Verlinde 2011) is ~ 0.6 and thus is inconsistent with the HW10 value of 0.35. Thus more research may be needed to arrive at a theoretically consistent formulation of ice fallspeeds that predicts fall speeds as accurately as the HW10 scheme.

From the above discussion, it follows that a comparison between the MH05 and the HW10 schemes would reveal some information about ice particle shape. For instance,

if the two schemes differ substantially from each other, the ice crystals may be open-branched planar crystals (e.g. stellar dendrites) or long columnar crystals. If percent differences are minor, it may be an indication that the ice crystals are compact or having aspect ratios near unity. It should be noted that fall speed computations for this paper use the HW10 formulation. The MH05 fall speed formulation is only used to compare fall velocity values of MH05 with HW10. In Fig. 1, V_m is predicted by both schemes using PSDs from anvil cirrus and synoptic cirrus. It can be seen that both schemes agree closely as indicated by the proximity of the regression line to the 1:1 line for both anvil and synoptic cirrus, where the fall speed predicted by HW10 is always slightly smaller (by 10% for the largest V_m) relative to MH05. Considering the Re representative of cirrus clouds in Fig. 2 of HW10 (Re from 1 to ~ 50), we may infer that the ice particle shapes observed during SPartICus were mostly compact ice particles having aspect ratios closer to unity (relative to long columns). This finding is similar to the remote sensing findings of van Diedenhoven et al. (2013) regarding aspect ratios of cirrus ice crystals. Further details on V_m computations and the data used in Fig. 1 are discussed under methodology in section 3.

3. Methodology

3.1. Field campaign

The SPartICus (Small PARTicles In CirrUS) field campaign was primarily designed to study the physical and dynamical characteristics of mid-latitude cirrus. As stated in the

science overview document for SPartICus by Mace et al. 2009, "Gathering representative statistics of cirrus microphysical properties is a major goal for SPartICus." One of the primary objectives of the SPartICus field campaign was to evaluate the concentrations of small ice crystals in cirrus clouds using new and improved instruments. These new instruments are much less vulnerable to ice particles shattering off of probe tips and inlet tubes compared to older aircraft instruments (Mace et al. 2009). The field campaign was conducted over the Southern Great Plains (SGP) site of the Atmospheric Radiation Measurement (ARM) program as well as along the tracks of satellite overpasses in the region (see Fig. 2) from January to June 2010.

3.2. Case study selection

Cirrus clouds sampled during SPartICus were grouped into anvil cirrus and synoptic cirrus based on satellite imagery and SPartICus flight notes. Here, fresh anvil cirrus follows the convention from Lawson et al. (2010), which refers to anvil cloud produced from deep convection that is still attached to its parent convection. Synoptic cirrus, also called cirrus clouds that are formed in situ, are formed by wide-spread vertical lifting in the upper troposphere. Anvil cirrus clouds are produced from deep convection with strong updrafts (~ 10 to 30 ms^{-1}), whereas the formation of synoptic cirrus is by large scale ascent with vertical velocities on the order of 10 to 30 cm s^{-1} and is unrelated to deep convection. Thus, synoptic cirrus clouds are characterized by ice formation conditions distinctly different from those of anvil cirrus. Previous studies (Connolly et al. 2005; Lawson et al. 2006b; 2010) show that ice particles in synoptic cirrus are predominantly rosette shaped, while fresh anvil cirrus is composed of a variety of habits,

but typically a dearth of rosette particles. Based on the above discussion, SPartICus flight days were divided into two groups, so that differences in the microphysical properties and fall speeds of anvil and synoptic cirrus could be compared. Cirrus clouds produced due to orographic lifting were not included in this study. Clouds that contained liquid water were excluded from the data set (see section 3.4 for details). Table 1 shows the classification of SPartICus flight days selected for this study.

3.3. Field Measurements

In-situ cloud data from the 2 Dimensional Stereo (2D-S) probe is used to get ice PSD in terms of number, area and mass concentration. The 2D-S consists of two diode laser beams that cross at right angles and illuminate two linear 128-photodiode arrays. These photodiode arrays work independently as high-speed and high-resolution optical imaging probes, producing shadowgraph images with true 10-μm pixel resolution at aircraft speeds up to 170 m s^{-1} (Lawson et al. 2006a).

The production of small ice crystals due to the shattering of large crystals on the inlets of aircraft particle measurement probes is now a well-known issue. Historical PSD measurements in cirrus clouds have been plagued by measurement uncertainties due to this shattering effect, resulting in artificially enhanced concentration of small ($D < 100$ μm) ice crystals (McFarquhar et al., 2007; Jensen et al., 2009; Lawson et al., 2010; Mitchell et al., 2010, Korolev et al., 2011). However, recent studies (Jensen et al. 2009; Lawson et al. 2010; Lawson 2011) have shown that the effect of shattering has been

greatly reduced in the new 2D-S probe that combines improved probe tip design, based on work reported in Korolev et al. (2011), with a particle arrival time shattering removal algorithm (Baker et al. 2009, Field et al. 2003, 2006; Lawson 2011). A recent study by Lawson (2011) using the 2D-S probe has revealed relatively high concentrations of small ice crystals near cloud top with decreasing concentration of small ice crystals toward cloud base. According to Lawson (2011), this is the first time that aircraft measurements from major field programs (e.g., SPartICus, TC4, MACPEX) show vertical profiles of ice particle concentration in deep ice clouds (anvils and deep cirrus) that are more consistent with physical arguments and numerical models. However, limited balloon-borne replicator sondes did suggest similar vertical profiles (Heymsfield and Miloschovich 1995).

In addition to the 2D-S probe, data from a Fast Forward Scattering Spectrometer Probe (FSSP) and the Cloud Particle Imager (CPI) were used to screen for liquid water described in section 3.4. Temperature measurements were made by a Rosemount total temperature probe. Atmospheric and aircraft state parameters were measured by the **A**ircraft- **I**ntegrated Meteorological Measurement System (AIMMS-20) probe mounted on the SPEC Learjet aircraft.

3.4. Data Selection and Quality Control

The cirrus cloud segments for this study were carefully selected to ensure adequate data quality was maintained. Cloud segments were identified by making sure

that they contained no liquid water, had good sampling statistics, and that the microphysical conditions during sampling were relatively stable. In order to ensure the criteria for good sampling statistics and stable microphysical conditions, the PSD data obtained from the 2D-S probe were processed as described below.

A sampled flight segment was initially accepted as a cloud segment when the extinction coefficient β_{ext} (twice the measured particle projected area) exceeds 0.1 km^{-1} over a 5 second period. Then the mean value of β_{ext} and the median mass dimension MMD (the ice particle maximum dimension separating the PSD mass into equal parts) are calculated over this period for a sample time resolution of 1 second (i.e. 1 Hz). If the maximum values of β_{ext} and MMD do not exceed their mean value by a factor of two, and their minimum values are not less than 0.4 times the mean value, then the segment is retained and the process continues. Sampling time is then increased in 1-second increments; every second the value of β_{ext} and MMD are calculated and compared against their respective cumulative mean values. If they do not exceed the threshold values described above, then the segment passes and another second is added. A segment must reach 60 seconds in length to be kept and when an accepted segment reaches 120 seconds in length the first half is cut off and kept as a separate PSD measurement segment (cloud segment) for analysis and the second half continues adding seconds provided the above criteria are met. The process continues until data for the entire flight is distributed into cloud segments that have sampling times between 60 and 120 seconds. The above approach makes use of a large portion of the data while ensuring relatively stable cloud conditions.

It was necessary to remove small patches of supercooled liquid water, which were typically encountered in clouds that did not qualify as anvil cirrus or synoptic cirrus. The selection process is intended to isolate ice-only conditions since the presence of liquid patches, although rarely encountered, can result in abrupt and large changes in number concentration, extinction and MMD. The following procedure was implemented to remove data containing liquid water.

1. Images from the CPI probe were manually assessed to ensure the absence of liquid water. The presence of numerous small spherical images was an indication for liquid. While small ($D < 50$ μm) ice crystals can often appear spherical or quasi-spherical, when liquid is present, spherical droplets overwhelm the CPI image, making the presence of liquid obvious. Such cloud segments were excluded from the data set.

2. Cloud particle concentrations from the fast FSSP and the 2D-S probe were analyzed. For a given cloud segment, if 1 second 2D-S data indicated a concentration of more than 3 particles per cubic centimeter or the FSSP probe indicated a concentration of more than 10 per cubic centimeter, the cloud segment was considered to have liquid and hence removed from the data set. However, SPartICus cloud segments rarely exceeded this threshold. Concentrations of ice particles in ice clouds generally range from 0.001 to 10 per cubic centimeter (e.g. Jensen et al. 2009, Mitchell et al. 2011c). In liquid clouds, the number concentrations are typically much higher, more than 20

per cubic centimeter (Lamb and Verlinde, 2011). Hence, the above thresholds for the 2DS and FSSP can effectively screen liquid water in clouds.

3. Cloud regions that were sampled at temperatures warmer than -20 °C were removed from the dataset. The number of samples in these relatively warm clouds were small (no more than 4 PSD for a five degree temperature interval) and may not be representative of cirrus conditions.

Implementation of the above data selection and quality control criteria resulted in 189 PSDs for synoptic cirrus and 108 PSDs for anvil cirrus that were grouped into 5°C temperature intervals ranging from -20°C to -65°C. A mean PSD was calculated for each temperature interval, producing 9 mean PSDs for synoptic and anvil cirrus. The number of PSDs selected in each temperature interval for anvil and synoptic cirrus are shown in Fig. 3.

3.5. Calculations

The mass weighted ice fall-speed or V_m was estimated directly from 2D-S in situ measurements of ice particle number, area and mass. These measurements yield the concentration of ice particle number and projected area for each size-bin of the measured PSD. The 2D-S also yields the estimated mass concentration (using the mass-area and mass-length relationships described in Baker and Lawson, 2006 and Lawson and Baker, 2006). From these measurements, the ice particle fall velocity v_t is calculated for each size-bin using the fall speed formulation of HW10. The treatment of V_m specific to the

2D-S probe has already been presented in Mitchell 2011b and hence is not repeated here (see equations 1 through 6 in Mitchell 2011b for details).

4. Results

4.1. Particle Size Distributions (PSDs)

Ice particle size distributions (PSDs) for anvil cirrus sampled during SPartICus are shown in Fig. 4. Similarly synoptic PSDs are shown in Fig. 5. There is a tendency for PSDs to evolve from narrow to broad with increasing temperature. This is expected if small ice particles are generated at colder temperatures and aggregation and diffusional growth occur as ice particles sediment. At temperatures warmer than – 40 ^{o}C, a distinct hump is exhibited by the PSDs in the neighborhood of 200 μm and may be indicative of aggregation.

4.2. Effective diameter (D_e)

The treatment of D_e in this study uses the universal definition for D_e (e.g. Mitchell 2002) and applies to all clouds irrespective of their phase. In this section, D_e is related to the temperature (T) of the cloud and the ice water content (IWC) for mid-latitude cirrus. D_e is very sensitive to the concentration of small ice crystals (Ivanova et al. 2001). As mentioned by McFarquhar et al., 2007; Jensen et al., 2009 and several others, in situ data from past measurements contained erroneously high concentrations of small crystals produced from ice crystal shattering on instrument probe inlets (Korolev et al. 2011; Lawson 2011). Hence, substantial reduction in shattering effects by the use of

2D-S data makes this relationship more reliable compared to past studies that used older cloud probes like the FSSP.

Fig. 6 shows the relationship of D_e to cloud temperature for anvil cirrus (left) and synoptic cirrus (right). The correlation coefficient for D_e-T relationship in SPartICus anvil cirrus was higher (r^2= 0.831) than synoptic cirrus (r^2= 0.676). Although temperature dependence is evident from the figure with smaller D_e values corresponding to colder temperatures, there is no statistically compelling evidence that the temperature dependence changes with the type of cirrus (anvil vs. synoptic).

Fig. 7 shows the relationship of D_e to IWC for anvil (left) and synoptic cirrus (right). As seen in the figure, the cloud type appears to affect the general relationship of D_e to IWC. The correlation coefficient for D_e-IWC relationship in SPartICus anvil cirrus was significantly higher (r^2= 0.7349) than synoptic cirrus (r^2= 0.3954). Moreover, the dependence of D_e on IWC is weaker than the dependence of D_e on T. Our results are similar to those reported in Liou et al. (2008) in finding a significant correlation between D_e and IWC, but our results differ in finding an even stronger correlation between D_e and temperature (the Liou et al. study found no significant correlation between D_e and temperature). This is further discussed in Mitchell et al. (2011b). The reason for the different results between studies is not entirely clear but may be related to the fact that the Liou et al. study used PSD data from probes not having the recent improvements that greatly reduce the problem of ice particle shattering.

Figs. 8(a) and 8(b) show a multiple variable regression relating D_e to T and IWC for anvil and synoptic cirrus, respectively. For De-T relationship, r^2 = 0.831 (anvil cirrus)

and $r^2 = 0.676$ (synoptic cirrus). Similarly for De-IWC relationship, $r^2 = 0.735$ (anvil cirrus) and $r^2 = 0.395$ (synoptic cirrus). Since D_e seemed to have good correlation with both T and IWC, both these variables were related to D_e. Multiple variable regression using both T and IWC resulted in a better correlation for both anvil ($r^2 = 0.8893$) and synoptic cirrus ($r^2 = 0.7359$) compared to using either T or IWC alone to predict D_e. This is particularly useful in predicting D_e for synoptic cirrus where the correlation coefficient increases significantly when both IWC and T are used to predict D_e. The wide range of cloud IWC (ranging from 1 mg m^{-3} to 1200 mg m^{-3}) made it necessary to represent IWC on a logarithmic scale resulting in the following relationship of D_e to T and IWC. The coefficients in Eq. 8 below are given in Table 2 for both anvil and synoptic cirrus:

$$D_e = a\,T + b \log (IWC) + c \qquad (8)$$

where D_e is expressed in micrometers, T is in ^{o}C and IWC is in mg m^{-3}.

4.3. Fall speed

In this section, the ice fall velocity is related to temperature and IWC. The ice fall speed depends on the ratio of ice particle mass to projected area while D_e depends on the ratio of IWC to projected area. Due to this common mass/area dependence, there is a strong correlation between D_e and V_m. Moreover, V_m is similarly correlated to T, IWC and combined T-IWC as is D_e.

In Fig. 9, V_m is related to T for anvil and synoptic cirrus. Similar to the D_e-T relationships, V_m-T relationships show a slightly stronger correlation for anvil cirrus ($r^2 = 0.783$) compared to synoptic cirrus ($r^2 = 0.659$). Fig. 10 shows the relationship of V_m to

IWC. Again, the correlation coefficients are similar to that between D_e and T. While r^2 is not as high as with the V_m-T relationship, it still explains more than 50% of the variance for anvil cirrus and about 40% of the variance for synoptic cirrus, suggesting a multiple regression using both T and IWC may be more powerful in diagnosing V_m. Hence, a multiple variable regression relating V_m to both IWC and T is presented in Fig. 11(a) for anvil cirrus and Fig. 11(b) for synoptic cirrus. It is seen that the use of both T and IWC to predict V_m results in an improvement in the regression statistics (r^2 = 0.85 and 0.73 for anvil and synoptic cirrus, respectively), similar to the results obtained for D_e. The following expression was obtained for relating V_m to T and IWC

$$V_m = a\,T + b\,\log(IWC) + c \qquad (9)$$

where V_m is in cm s^{-1}, T is in °C, and IWC is in mg m^{-3}. The above coefficients are given in Table 2 for anvil and synoptic cirrus. V_m computed using Eq. 9 and the coefficients in Table 2 (for both synoptic and anvil cirrus) tend to have negative values when T < -65 ^oC and IWC < 1 mg m^{-3} since the selected SPartICus case studies did not have measurements beyond these values of T and IWC. The lowest values of V_m in SPartICus cirrus are from 2-4 cm s^{-1}. Thus, it is suggested that a lower bound (e.g. V_m = 1 cm s^{-1}) or alternate expression for V_m be used when models need to predict V_m based on IWC and T for T < -65 ^oC and IWC < 1 mg m^{-3}.

These results indicate that T and IWC can be used to predict V_m diagnostically in climate models, or they can also be used to test V_m predicted in various model microphysics modules. The fairly robust relationship between V_m and (T, IWC) may provide a rigorous test for relating climate models to observations.

4.4. Comparison of SPartICus Fall Speed with Doppler Derived Fall Speeds From Deng And Mace 2008

In this section, the ice fall velocity obtained from SPartICus data using the HW10 scheme is compared with ice fall velocities obtained by Deng and Mace 2008 (DM08) using cloud radar Doppler moments. DM08 applied a cirrus cloud retrieval algorithm (Deng and Mace 2006) to a 7-year record of millimeter cloud radar (MMCR) data collected at two ARM sites: Southern Great Plains (SGP) of the United States and the tropical western Pacific (TWP), which includes the islands of Manus and Nauru. DM08 used data collected from 1999 through 2005 in isolated layers where ice microphysical processes were dominant. The data set was comprised of about 30,000 hours of remotely sampled cirrus data from these sites. Since SPartICus data is obtained from cirrus over the ARM SGP site, the results from this study are compared with the SGP retrievals of V_m, IWC and T in DM08. DM08 related V_m to T and IWC using the following formulation; the coefficients of this equation are given in Table 3:

$$\log(V_m) = a\, T^2 \log(IWC) + b\, T \log(IWC) + c \log(IWC) + d\, T + e\,. \qquad (10)$$

Using the above equation and the coefficients in DM08 for SGP cirrus, the V_m predicted from (10) using the SPartICus temperature and IWC measurements was compared against the V_m computed from 2D-S measurements of ice particle mass and area (2D-S derived V_m) during SPartICus (Fig. 12 A and B). It is seen that although there is good correlation between V_m predicted by the MMCR and the 2D-S derived V_m, the results deviate from the 1:1 line. In Fig. 12 (C and D), the terms (i.e. mathematical operations) used in the DM08 equation were used with corresponding coefficients derived from this

SPartICus data. This approach resulted in better correlation since both the coefficients and the data are from SPartICus.

In Fig. 11 (A and B), the simplest expression relating V_m to T and IWC, as in Eq. (9), was used to predict V_m and was compared against the 2D-S derived V_m. Comparing the regression in Fig. 12 (C and D) with the regression in Fig. 11 (A and B) shows that no significant improvement was achieved by using additional T and IWC terms to predict V_m. Hence, the simplest method using only the log(IWC) and T terms (i.e. Eq. 9) was adopted to compare the results of this study with that of DM08.

The DM08 Eq. 10 is contrasted with Eq. 9 in Fig. 13 (A) for synoptic cirrus data at three temperatures roughly spanning the range of SPartICus measurements. The curves resulting from Eq. 9 and 10 are similar where SPartICus measurements are abundant but curves using Eq.10 diverge from Eq. 9 curves near the limits of the SPartICus data domain, with (10) showing less dependence on temperature. Similar results were also seen for anvil cirrus (not shown). Figs. 13 (B, C and D) compare equation (9) with (10) at three temperatures where SPartICus data density was higher. V_m derived from in situ measurements, given by the circle symbols, were compared against the two V_m parameterizations. For synoptic cirrus, measurement derived V_m-IWC-T values correspond to temperature intervals of -25°C to -28°C, -41°C to -43°C, and -55°C to -57°C, respectively.

The comparison of this scheme with the DM08 scheme shows that the DM08 results violate the 1:1 lines in Fig. 12 A & B although they have good correlation with observations. The difference in the slope of the regression line compared to the 1:1 line

indicates the presence of a bias in the DM08 scheme. A recent paper by Borg et al. 2011 demonstrated that the MMCR fails to detect optically thin cirrus (optical depth < 0.2) and is often not sensitive to the complete vertical extent of the cloud which may partly explain the bias in the DM08 scheme. By using extinction profiles from a Raman Lidar over the multi-year record, they also found that the MMCR missed about 30% of the total cloud optical depth near the cloud top, and nearly 40% of the optically thinnest cirrus clouds.

Fig. 13 A also shows that the DM08 scheme is less sensitive to temperature than our scheme. Panels B and D in this figure further illustrate this and show that our scheme better conforms to the data, with the DM08 scheme underestimating V_m at warmer temperatures and overestimating V_m at colder temperatures. Mitchell et al. (2011b) performed a similar comparison to the DM08 scheme and found that DM08 was comparatively less sensitive to T for tropical anvil cirrus. However, the results from Mitchell et al. (2011b) had much better agreement with the DM08 scheme, which may be due to the fact that narrow T intervals of high data density were not available near the dataset temperature boundaries in that case. It could also indicate that the MMCR retrieval biases were reduced for the tropical western Pacific dataset. It should also be noted that the fall speeds predicted from the Deng and Mace scheme do not converge to zero for really small values of IWC and stay above 20 cm s^{-1}. This is especially true at colder temperatures. V_m predicted using SPartICus data converge to zero for low values of IWC, which is physically more reasonable.

Despite the above dissimilarities between the results from this scheme and the DM08 scheme, it should be noted that the estimates of fall speed from both the schemes are generally in good-to-fair agreement with each other. The fact that these two schemes result from completely different measurement techniques provides some measure of confidence that we are making progress in estimating the ice fall speed. These results suggest that V_m in cirrus clouds can now be realistically estimated in terms of T and IWC.

4.5. Relating V_m to D_e

Enhanced coupling in climate models between the ice cloud microphysics (which should govern V_m), the ice cloud optical properties (which are generally predicted from D_e and IWC) and the predicted cloud radiative forcing (which depends on both D_e and V_m) can be accomplished by expressing V_m in terms of D_e, provided that D_e is predicted by the microphysics module and is then passed to the radiation component of the model (Mitchell et al. 2011b). The mathematical similarity in the formulation of D_e and V_m results in strong correlations between the two variables and further supports this approach. The relationship between D_e and V_m is shown in Fig. 14 for both anvil and synoptic cirrus sampled during SPartICus, and it assumes a temperature of -20°C and a pressure of 500 hPa. A second order polynomial fit resulted in a very strong correlation between V_m and D_e for both kinds of cirrus with r^2 values greater than 0.98. However, it produced a negative intercept that gives non-physical (i.e. negative) values of V_m for $D_e <$ 12 μm (anvil cirrus only). This limitation may arise because at smaller sizes, viscous flow dominates and V_m is likely to conform more to Stokes law (M96), which diverges

from the observed relationship that is based on different flow regimes. To adjust for this, the regression line was forced through the origin (for both anvil and synoptic cirrus) and the following relationship was obtained for anvil cirrus for all values of D_e:

$$V_m = 0.0047\ D_e^2 + 0.0678\ D_e\ . \qquad (11)$$

Similarly for synoptic cirrus,

$$V_m = 0.0049\ D_e^2 + 0.0187\ D_e\ . \qquad (12)$$

In the above equations, the unit for V_m is cm s^{-1} and the unit for D_e is μm.

Strong correlations between V_m and D_e have also been observed in other studies like Mitchell et al. (2011b) and Heymsfield et al. (2003). The recent study by Mitchell et al. (2011b) related V_m to D_e for tropical cirrus and Arctic cirrus. In both cases, a strong positive correlation ($r^2 > 0.9$) was found between V_m and D_e. Based on these results, D_e can be considered a very good parameter to predict V_m in GCMs.

5. Summary and Conclusions:

The use of the 2D-S probe in this study has resulted in new findings and has enabled better estimation of D_e and V_m in mid-latitude cirrus. The use of multiple variable regressions to predict V_m and D_e by combining T and IWC resulted in a significant improvement compared to individually using T or IWC to predict V_m and D_e. The cloud temperature (T) exhibited a higher correlation with V_m and D_e compared to IWC. Climate models using single-moment microphysical schemes can be improved by

relating the variables temperature and ice mixing ratio (i.e. IWC) to V_m, as shown in this study. In situations where a diagnostic prediction of V_m is not preferred, the fairly robust relationship between V_m and (T, IWC) may provide a means of testing climate model predictions of V_m. However, if climate models using two-moment microphysical schemes predict V_m in terms of T and IWC only, it may mask some of the physical coupling between the cloud microphysical and optical properties since, in addition to ice mass, V_m is dependent on the PSD projected area that cloud optical properties also depend on.

For climate models using two-moment microphysical schemes, Fig. 15 shows an improved way of predicting cloud feedback and climate sensitivity based on Section 4.5. In Fig. 15, information regarding aerosols and other environmental parameters (e.g. pressure, temperature, cloud updraft, etc.) is supplied to the cloud microphysics module of a climate model that uses this information to compute V_m from D_e based on Eqs. 11 and 12. The cloud microphysics module also supplies information regarding IWC to predict V_m and D_e. This information is used to compute the ice mass flux ($V_m \times$ IWC), which is essential for determining the cloud life cycle, cloud coverage and upper tropospheric (UT) water vapor. Values of D_e and IWC are provided to the cloud optical properties module that uses this information to compute cloud optical depth, single scattering albedo and asymmetry parameter. Information from the optical properties module is then combined with information regarding cloud coverage, IWC, ice water path (related to cloud life cycle) and UT water vapor to help predict cloudy and clear-sky radiative forcing and cloud feedback, which are known to affect climate sensitivity. It is

expected that such a treatment of V_m and D_e would produce results that are more consistent with that of the real world.

Favorable agreement was generally found between our measurement derived values of V_m, IWC and T and those predicted by a V_m parameterization based on cloud Doppler radar retrievals of IWC and V_m (Deng and Mace 2008). However, the Deng and Mace scheme suffered from lack of sensitivity to cloud temperature, underestimating V_m at warmer temperatures and seriously overestimating V_m at colder temperatures.

Although a fairly robust relationship is found between V_m and (T, IWC), predicting V_m from D_e is found to be superior ($r^2 > 0.98$). The strong correlation between V_m and D_e is also supported by previous studies (Heymsfield 2003 and Mitchell et al. 2011b). V_m is strongly correlated with D_e owing to a common dependence of both these parameters on the ice particle mass-to-area ratio. In a study by Mitchell et al. (2008), D_e, V_m and the ice optics in cirrus clouds were derived from temperature-dependent PSD schemes and thus physically coupled in the NCAR Community Atmospheric Model, version 3 (CAM3), revealing a strong impact of V_m on model climatology that was otherwise less evident. In two-moment ice microphysical schemes that predict both the ice mixing ratio and number concentration, D_e is often predicted based on the IWC and PSD projected area, which require assumptions about the PSD and ice particle shape. Thus, predicting V_m from D_e in two-moment microphysical schemes also provides self-consistency between V_m, D_e and assumptions about the PSD and ice particle shape. By implementing this method, the coupling between the ice microphysics and radiation is

unambiguous, assuming that D_e is determined by the microphysics and then used to calculate cloud optical properties.

Acknowledgements

This research was supported by the Office of Science (BER), U.S. Department of Energy. Additional support was obtained through NSF EPSCoR grant EPS-0814372. The authors are grateful to the scientists at SPEC Inc. for their help and support during the data analysis process. Dr. Qixu Mo is sincerely acknowledged for providing Matlab code for initial data processing. We thank Dr. Brad Baker for answering numerous scientific and field data related questions. We also thank Dr. Sara Lance at SPEC for reprocessing the initial SpartICus data with a corrected algorithm intended for our specific needs.

References

Baker, B., and R. P. Lawson (2006), Improvement in determination of ice water content from two-dimensional particle imagery. Part I: Image-to-mass relationships. *J. Appl. Meteor. Climatol., 45*, 1282-1290, 2006.

Baker, B. A., A. Korolev, R. P. Lawson, D. O'Connor, Q. Mo, Q. (2009), Drop Size Distributions and the Lack of Small Drops in RICO Rain Shafts, J. Appl. Meteorol., 48, 616–623.

Bohm, H. P. (1989), A general equation for the terminal fall speed of solid hydrometeors. *J. Atmos. Sci.,* **46,** 2419–2427.

Bohm, H. P. (1992), A general hydrodynamic theory for mixed-phase microphysics. Part I: Drag and fall speed of hydrometeors. *Atmos. Res.,* **27,** 253–274.

Borg, L. A., R. E. Holz, and D. D. Turner (2011), Investigating cloud radar sensitivity to optically thin cirrus using collocated Raman lidar observations, Geophys. Res. Lett., 38, L05807, doi:10.1029/2010GL046365.

Connolly, P.J., C.P.R. Saunders, M. W. Gallagher, K. N. Bower, M. J. Flynn, T. W. Choularton, J. Whiteway, R. P. Lawson (2005), Aircraft observations of the influence of electric fields on the aggregation of ice crystals, *Q. J. Roy. Meteorol. Soc.,* **18**, 1695-1712.

Deng, M., and G. Mace (2006), Cirrus microphysical properties and air motion statistics using cloud radar Doppler moments. Part I: Algorithm description. J. Appl. Meteor. Climatol., **45,** 1690– 1709.

Deng, M. and G. G. Mace, (2008), Cirrus cloud microphysical properties and air motion statistics using cloud radar Doppler moments, (2008), Water content, particle size, and sedimentation relationships, *Geophys. Res. Lett., 35,* L17808, doi:10.1029/2008GL035054.

Field, P. R., R. Wood, P. R. A Brown, P. H. Kaye, E. Hirst, R. Greenaway, J. A. Smith (2003), Ice particle interarrival times measured with a Fast FSSP, J. Atmos. Oceanic Technol., 20, 249– 261.

Field, P. R., A. J. Heymsfield, and A. Bansemer (2006), Shattering and Particle Interarrival Times Measured by Optical Array Probes in Ice Clouds, J. Atmos. Oceanic Technol., 23, 1357–1370.

Heymsfield, A.J. and L.M. Miloshevich (1995), Relative humidity and temperature influences on cirrus formation and evolution: Observations from wave clouds and FIRE II, *J. Atmos. Sci.*, **52**, 4302-4326.

Heymsfield, A. J. (2003), Properties of tropical and midlatitude ice cloud particle ensembles. Part II: Applications for mesoscale and climate models, *J. Atmos. Sci., 60*, 2592-2611.

Heymsfield, A. J., S. Matrosov, and B. A. Baum (2003), Ice water path–optical depth relationships for cirrus and precipitating cloud layers. *J. Appl. Meteor.*, **42,** 1369–1390.

Heymsfield, A. J., A. Bansemer and C. Twohy (2007), Refinements to ice particle mass dimensional and terminal velocity relationships for ice clouds. Part I: Temperature dependence. *J. Atmos. Sci., 64*, 1047-1067.

Heymsfield, A. J. and C. Westbrook (2010), Advances in the estimation of ice particle fall speeds using laboratory and field measurements, *J. Atmos. Sci., 67*, 2469-2482, 2010.

Ivanova, D.C., D.L. Mitchell, W.P. Arnott and M. Poellot (2001), A GCM parameterization for bimodal size spectra and ice mass removal rates in mid-latitude cirrus clouds, *Atmos. Res.*, *59*, 89-113, 2001.

Jensen, E. J., P. Lawson P., B. Baker, B. Pilson, Q. Mo, A. Heymsfield, A. Bansemer, T. Bui, M. McGill, D. Hlavka, G. Heymsfield, S. Platnick, G. T. Arnold, and S. Tanelli (2009), On the importance of small ice crystals in tropical anvil cirrus. *Atmos. Chem. Phys.*, Vol.9, No. 15, pp. 5519-5537, ISSN 1680-7316.

Korolev, A. V., E. F. Emery, J. W. Strapp, S. G. Cober, G. A. Isaac, M. Wasey, and D. Marcotte (2011), Small ice particles in tropospheric clouds: Fact or Artifact? Airborne Icing Instrumentation Evaluation Experiment, Evaluation Experiment. *Bull. Amer. Meteor. Soc.*, **92**, 967–973. doi: http://dx.doi.org/10.1175/2010BAMS3141.1

Lamb D., J. Verlinde (2011): Physics and Chemistry of Clouds. Cambridge University Press, New York. ISBN 978-0-521-89910-9

Lawson, R. P. and B., Baker (2006), Improvement in Determination of Ice Water Content from Two-Dimensional Particle Imagery. Part II: Applications to Collected Data. *J. Appl. Meteor. Climatol., 45*, 1291-1303.

Lawson, R. P., D. O'Connor, P. Zmarzly, K. Weaver, B. Baker, Q. Mo, and H. Jonsson (2006a), The 2D-S (Stereo) Probe: Design and preliminary tests of a new airborne, high-speed, high-resolution particle imaging probe. J. Atmos. Oceanic Technol., Vol.23, No.11, pp. 1462-1477, ISSN 1520-0426.

Lawson, R. P., B. A. Baker, B. Pilson, Q. Mo (2006b), In Situ observations of the microphysical properties of wave, cirrus and anvil clouds. Part II: Cirrus Clouds. *J. Atmos. Sci*., **63**, 3186-3203.

Lawson, R. P., E. Jensen, D. L. Mitchell, B. Baker, Q. Mo, and B. Pilson (2010), Microphysical and radiative properties of tropical clouds investigated in TC4 and NAMMA, J. Geophys. Res., 115, D00J08, doi:10.1029/2009JD013017.

Lawson, R.P. (2011), Effect of ice particles shattering on the 2D-S probe, Atmos. Meas. Tech., 4, 1361–1381, doi:10.5194/amt-4-1361-2011.

Liou, K. N., Y. Gu, Q. Yue and G. McFarguhar (2008), On the correlation between ice water content and ice crystal size and its application to radiative transfer and general circulation models, Geophys. Res. Lett., 35, L13805, doi:10.1029/2008GL033918.

Mace, J., E. Jensen, G. McFarquhar, G., J. Comstock, T. Ackerman, D. Mitchell, X. Liu, and T. Garrett (2009), "SPartICus: Small particles in cirrus science and operations plan." *Publications (E).* Paper 33. http://digitalcommons.library.unlv.edu/renew_pubs/33

McFarquhar, G. M., and A. J. Heymsfield (1997), Parameterization of tropical cirrus ice crystals size distributions and implications for radiative transfer: Results from CEPEX, J. Atmos. Sci., 54, 2187–2200.

McFarquhar, G. M., and co authors (2007), Ice properties of single-layer stratocumulus during the Mixed-Phase Arctic Cloud Experiment: 1. Observations. *J. Geophys. Res.*, VOL. 112, D24201, doi:10.1029/2007JD008633.

Mitchell, D.L. (1996), Use of mass- and area-dimensional power laws for determining precipitation particle terminal velocities. *J. Atmos. Sci.,* **53,** 1710–1723.

Mitchell, D.L. (2002), Effective diameter in radiation transfer: General definition, applications and limitations, J. Atmos. Sci., 59, 2330-2346.

Mitchell, D. L., and A. J. Heymsfield (2005), Refinements in the treatment of ice particle terminal velocities, highlighting aggregates. *J. Atmos. Sci.*, *62*, 1637-1644.

Mitchell, D.L., P. Rasch, D. Ivanova, G.M. McFarquhar and T. Nousiainen (2008), Impact of small ice crystal assumptions on ice sedimentation rates in cirrus clouds and GCM simulations. *Geophys. Res. Lett.*, **35**, L09806, doi:10.1029/2008GL033552.

Mitchell, D. L. and W. Finnegan (2009), Modification of cirrus clouds to reduce global warming. *Environ. Res. Lett.*, Vol.4, 045102, (October 2009), pp. 1-8, ISSN 1748-9326.

Mitchell, D.L., R.P. Lawson, and B. Baker (2011), Understanding effective diameter and its application to terrestrial radiation in ice clouds. Atmos. Chem. Phys., 11, 3417-3429, doi:10.5194/acp-11-3417-2011.

Mitchell, D. L., S. Mishra, and R. P. Lawson (2011**b),** Representing the ice fall speed in climate models: Results from Tropical Composition, Cloud and Climate Coupling (TC4) and the Indirect and Semi-Direct Aerosol Campaign (ISDAC), J. Geophys. Res., 116, D00T03, doi:10.1029/2010JD015433.

Mitchell, D. L., S. Mishra and R. P. Lawson (2011c), Cirrus clouds and climate engineering: New findings on ice nucleation and theoretical basis. In: *Planet Earth 2011 - Global Warming Challenges and Opportunities for Policy and Practice*, Prof. Elias Carayannis (Ed.), ISBN 978-953-307-733-8, InTech, Available from <http://www.intechopen.com/articles/show/title/cirrus-clouds-and-climate-engineering-new-findings-on-ice-nucleation-and-theoretical-basis>

Morrison, H. and A. Gettelman (2008), A new two-moment bulk stratiform cloud microphysics scheme in the community atmosphere model, version 3 (CAM3). Part I: Description and numerical tests. *J. Climate*, *21*(15): 3642-3659, doi: 10.1175/2008JCLI2105.1.

Pruppacher, H. R., and J. D. Klett (1997), Microphysics of Clouds and Precipitation. 2nd ed. Kluwer Academic, 954 pp.

Sanderson, B.M., C. Piani, W.J. Ingram, D.A. Stone, M.R. Allen (2008), Towards constraining climate sensitivity by linear analysis of feedback patterns in thousands of perturbed-physics GCM simulations. *Clim. Dyn.*, **30**, 175-190.

Sanderson, B. M. (2011), A Multimodel Study of Parametric Uncertainty in Predictions of Climate Response to Rising Greenhouse Gas Concentrations, *Journal of Climate*, Volume 24, Issue 5, pp. 1362-1377, doi: 10.1175/2010JCLI3498.1

Stephens, G. L. (2005), Cloud feedbacks in the climate system: A critical review. *J. Climate,* **18,** 1149–1152.

Twohy, C. H., A. J. Schanot, and W.A. Cooper (1997), Measurement of condensed water content in liquid and ice clouds using an airborne counter-flow virtual impactor. *J. Atmos. Oceanic Technol.*, Vol.14, No.1, pp. 197-202, ISSN 1520-0426. Perspective

Twohy, C. H., J. W. Strapp, and M. Wendisch (2003), Performance of a counterflow virtual impactor in the NASA icing research tunnel. *J. Atmos. Oceanic Technol.*, Vol.20, No. 6, pp. 781-790, ISSN 1520-042.

Van Diedenhoven, B., B. Cairns, A. M. Fridlind, A. S. Ackerman and T. J. Garrett (2013), Remote sensing of ice crystal asymmetry parameter using multi-directional polarization measurements – Part 2: Application to the Research Scanning Polarimeter. *Atmos. Chem. Phys.*, **13**, 3185–3203.

List of Table Captions:

Table 1. Case studies selected for SPartICus flights and their classification as anvil or synoptic cirrus.

Table 2. Coefficients used in Eq. 9 and 10 for relating D_e and V_m to IWC and temperature, based on in-situ measurements from SPARICUS synoptic and anvil clouds.

Table 3: Coefficients used in Eq. 11 for relating D_e and V_m to IWC and temperature. The first column shows the coefficients used in Deng and Mace (2008) for their V_m formulation, based on cloud radar observations at the ARM SGP site. The second and third columns of coefficients are obtained by using Eq. 11 for SPartICus derived V_m. Units for D_e, V_m, T and IWC are microns, cm s^{-1}, °C and mg m^{-3} for SPartICus and are cm s^{-1}, °C and g m^{-3} in Deng and Mace 2008 study.

List of Figure Captions:

Figure 1: Comparison of V_m calculated using the Mitchell and Heymsfield (2005) scheme (MH05) with V_m using the Heymsfield and Westbrook (2010) scheme (HW10) to infer ice particle shape information.

Figure 2. Flight operations area includes two 400-nautical-mile circles centered around Boulder, Colorado, and the ARM SGP site near Lamont, Oklahoma. Figure from SPartICus Science Overview by Mace et al. (2009).

Figure 3. Sampling statistics for anvil cirrus (top) and synoptic cirrus (bottom) cloud segments from the SPartICus field campaign based on temperature intervals of 5°C.

Figure 4. Temperature dependence of ice PSDs in SPartICus anvil cirrus for temperature ranging from -20 ^{o}C to -65 ^{o}C. Note that solid lines indicate PSDs for temperatures warmer than the homogeneous nucleation threshold (-40 ^{o}C). Dashed lines represent PSDs for temperatures colder than -40 ^{o}C.

Figure 5. Temperature dependence of ice PSDs in SPartICus synoptic cirrus for temperature ranging from -20 ^{o}C to -65 ^{o}C. Note that solid lines indicate PSDs for temperatures warmer than the homogeneous nucleation threshold (-40 ^{o}C). Dashed lines represent PSDs for temperatures colder than -40 ^{o}C.

Figure 6. Temperature dependence of D_e for anvil and synoptic cirrus sampled during SPartICus.

Figure 7. Dependence of D_e on ice water content (IWC) for anvil and synoptic cirrus in SPartICus. N denotes the number of PSDs for the type of cirrus.

Figure 8(a). Multiple variable regression predicting D_e in terms of temperature and IWC for SPartICus anvil cirrus.

Figure 8(b). Multiple variable regression predicting D_e in terms of temperature and IWC for SPartICus synoptic cirrus data.

Figure 9. Temperature dependence of V_m for anvil and synoptic cirrus clouds. N denotes the number of PSDs for each type of cirrus.

Figure 10. Dependence of V_m on ice water content (IWC) for anvil and synoptic cirrus during SPartICus.

Figure 11(a). Multiple variable regression to predict V_m in terms of temperature and IWC for SPartICus anvil cirrus.

Figure 11(b). Multiple variable regression to predict V_m in terms of temperature and IWC for SPartICus synoptic cirrus.

Figure 12. Predicting V_m in terms of temperature and IWC using the formulation of Deng and Mace 2008 (Eq. 12) for SPartICus anvil and synoptic cirrus. A and B are produced by using coefficients derived for SGP cirrus by Deng and Mace 2008. C and D are produced by using coefficients derived from SPartICus data and using the relationship of V_m to T and IWC as derived by Deng and Mace 2008.

Figure 13. Prediction of mass-weighted fall-speed (V_m) in terms of cloud temperature and IWC, based on Eq. 11 (black curves) and the V_m scheme of Deng and Mace (red curves) spanning the approximate temperature range of synoptic cirrus sampled in SPartICus. (b) Same but for T = -27°C, comparing measurement derived V_m from -25°C to -28°C; (c) same but for T = -42°C,

comparing V_m from -41°C to -43°C; (d) same but for T = -56°C, comparing V_m from -55°C to -57°C.

Figure 14. Predicting V_m from D_e for SPartICus anvil cirrus (top) and synoptic cirrus (bottom) using the HW10 formulation. Note that in both the figures, $R^2 > 0.98$.

Figure 15. Model consistency diagram suggesting the best way to parameterize V_m to improve the prediction of climate sensitivity. V_m is expressed in terms of D_e, provided that D_e is predicted by the microphysics module and then passed on to the radiation component of the model.

SPartICus Synoptic Cirrus Cases	SPartICus Anvil Cirrus Cases
1. Jan 19th, 2010 (Flight A)	1. April 22nd, 2010 (Flight A)
2. Jan 20th, 2010 (Flight A & B)	2. April 28th, 2010 (Flight A & B)
3. Jan 26th, 2010 (Flight A)	3. June 12th, 2010 (Flight A & B)
4. Jan 27th, 2010 (Flight A)	4. June 14th, 2010 (Flight A)
5. Feb 11th, 2010 (Flight A & B)	5. June 15th, 2010 (Flight A)
6. March 23rd, 2010 (Flight A, B & C)	6. June 24th, 2010 (Flight A & B)
7. March 26th, 2010 (Flight A)	
8. April 1st, 2010 (Flight A & B)	

Table 1. Case studies selected for SPartICus flights and their classification as anvil or synoptic cirrus.

Coefficient	Anvil D_e	Synoptic D_e	Anvil V_m	Synoptic V_m
a	1.631	1.759	1.119	1.411
b	17.96	13.49	14.21	11.71
c	124.4	139.7	68.85	82.35

Table 2. Coefficients used in Eq. 9 and 10 for relating D_e and V_m to IWC and temperature, based on in-situ measurements from SPartICus synoptic and anvil clouds. Temperature range is from -20 °C to -65 °C.

Coefficient	DM08 (SGP)	Anvil V_m (using DM08 equation)	Synoptic V_m (using DM08 equation)
a	-1.70704e-5	0.0405	0.0286
b	-3.19109e-3	-0.3691	-0.4242
c	-1.69876e-2	-0.0138	-0.022
d	4.10839e-3	4.816e-5	1.787e-4
e	1.93644	2.8434	2.5003

Table 3: Coefficients used in Eq. 11 for relating D_e and V_m to IWC and temperature. The first column shows the coefficients used in Deng and Mace (2008) for their V_m formulation, based on cloud radar observations at the ARM SGP site. The second and third columns of coefficients are obtained by using Eq. 11 for SPartICus derived V_m. Units for D_e, V_m, T and IWC are microns, cm s^{-1}, °C and mg m^{-3} for SPartICus and are cm s^{-1}, °C and g m^{-3} in Deng and Mace 2008 study. Temperature range is from -20 °C to -65 °C.

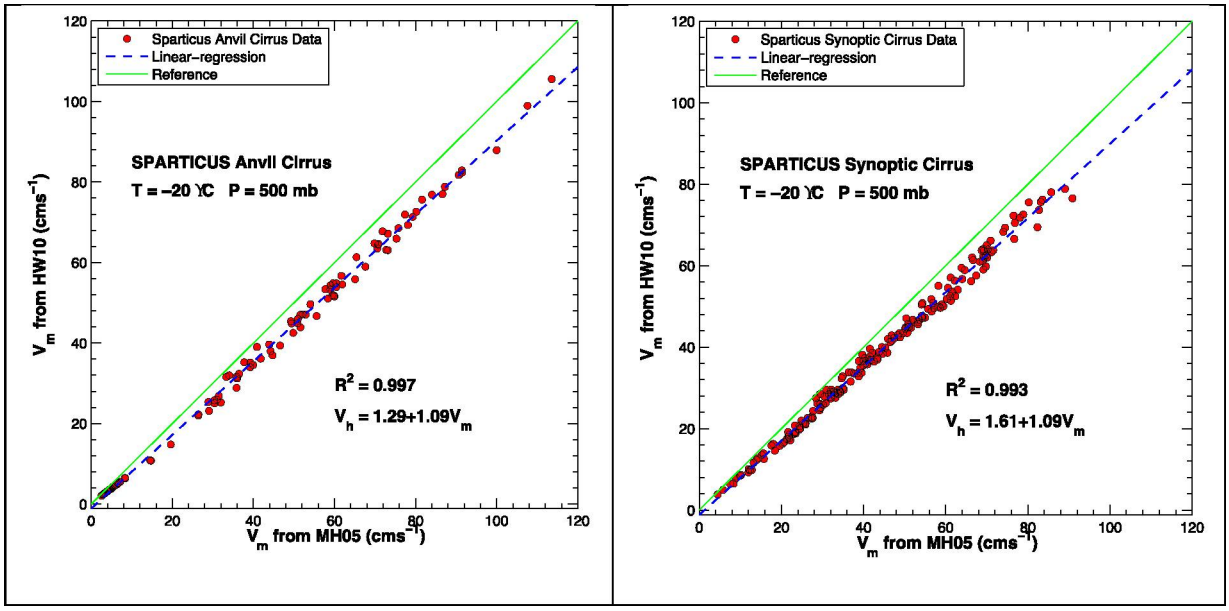

Figure 1: Comparison of V_m calculated using the Mitchell and Heymsfield (2005) scheme (MH05) with V_m using the Heymsfield and Westbrook (2010) scheme (HW10) to infer ice particle shape information.

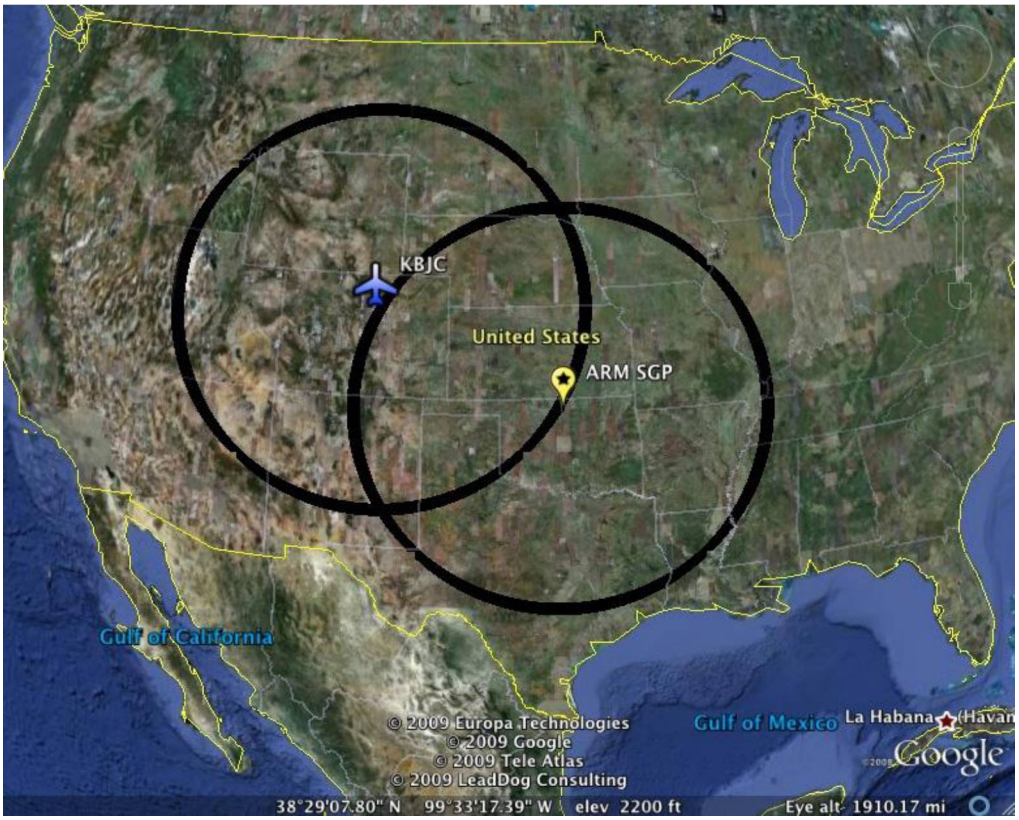

Figure 2. Flight operations area includes two 400-nautical-mile circles centered around Boulder, Colorado, and the ARM SGP site near Lamont, Oklahoma. Figure from SPartICus Science Overview by Mace et al. (2009).

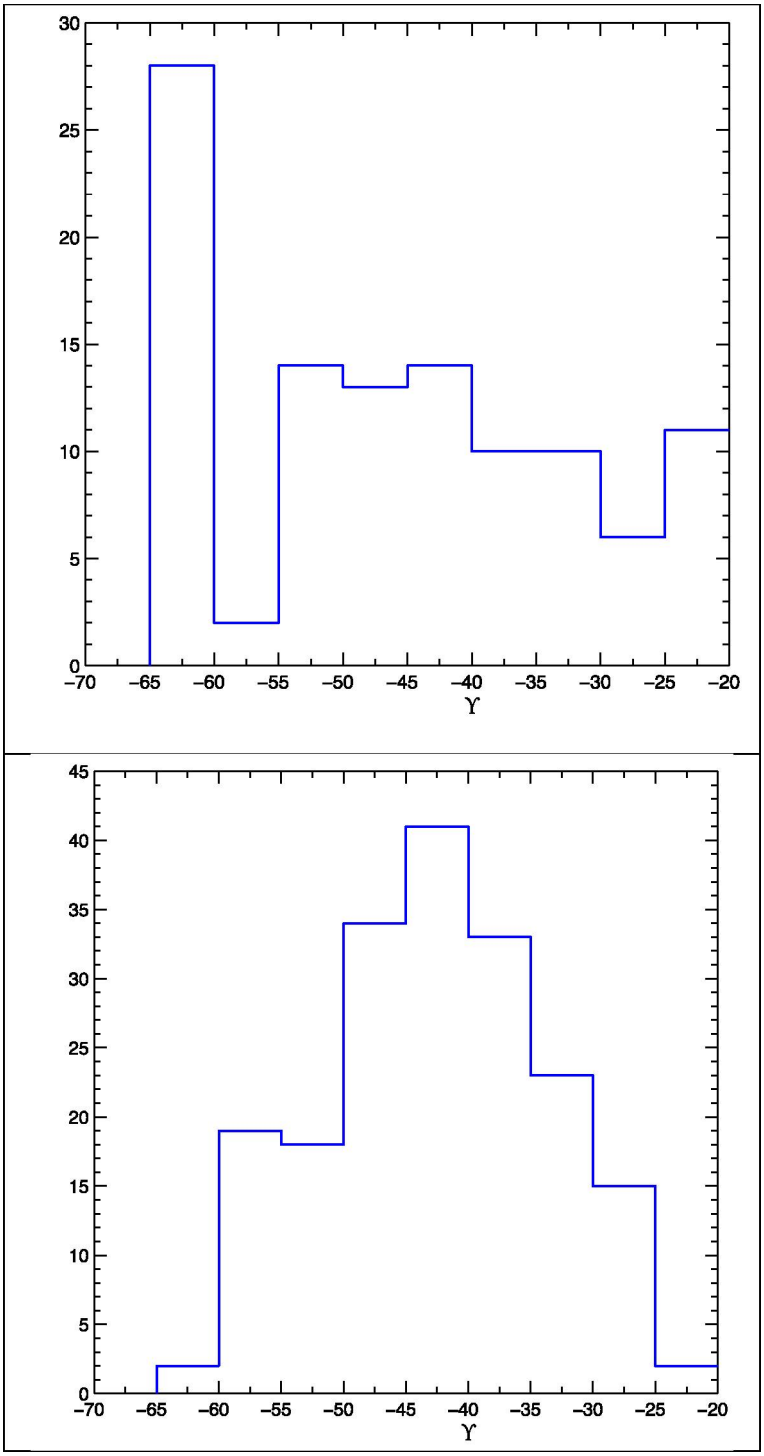

Figure 3. Sampling statistics for anvil cirrus (top) and synoptic cirrus (bottom) cloud segments from the SPartICus field campaign based on temperature intervals of 5°C.

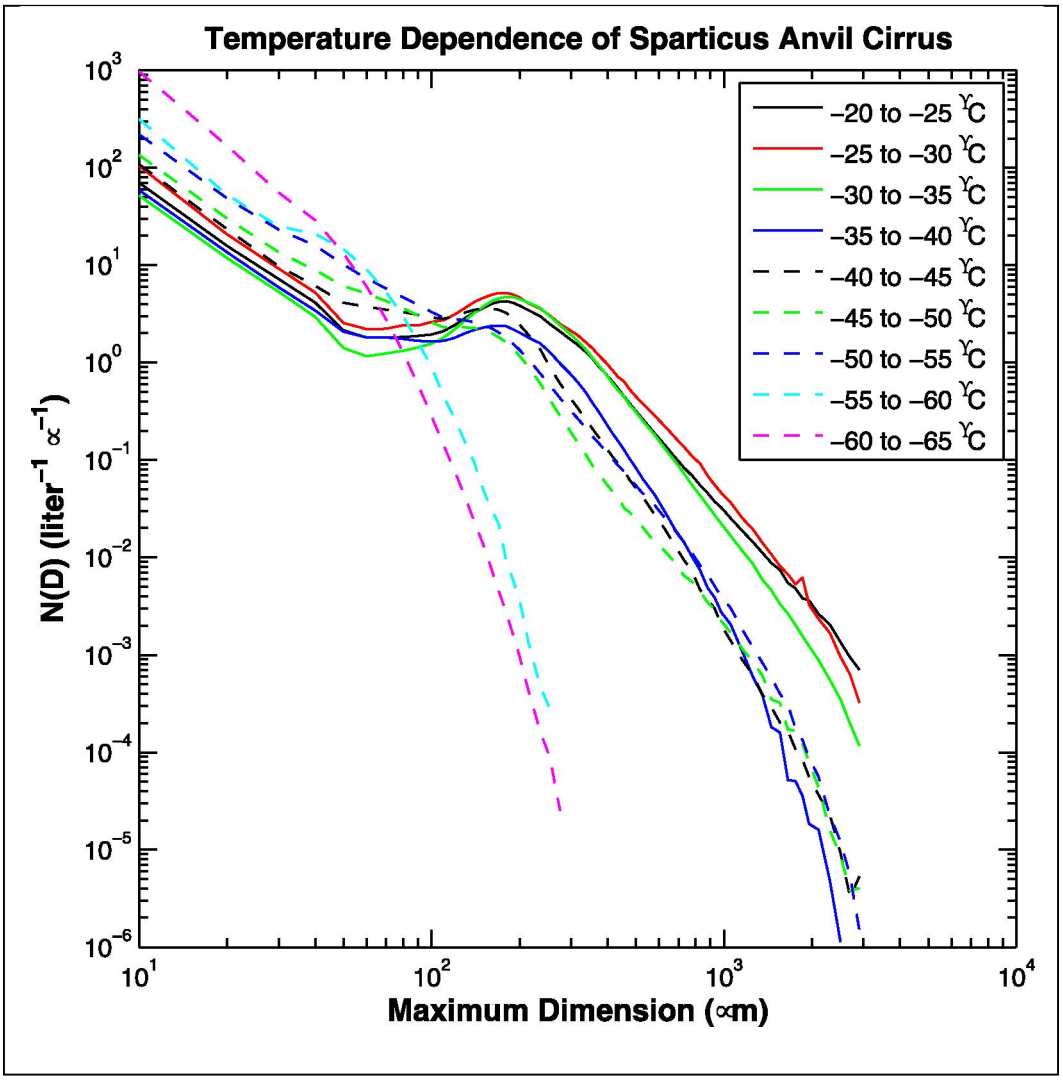

Figure 4. Temperature dependence of ice PSDs in SPartICus anvil cirrus for temperature ranging from -20 °C to -65 °C. Note that solid lines indicate PSDs for temperatures warmer than the homogeneous nucleation threshold of (-40 °C). Dashed lines represent PSDs for temperatures colder than -40 °C.

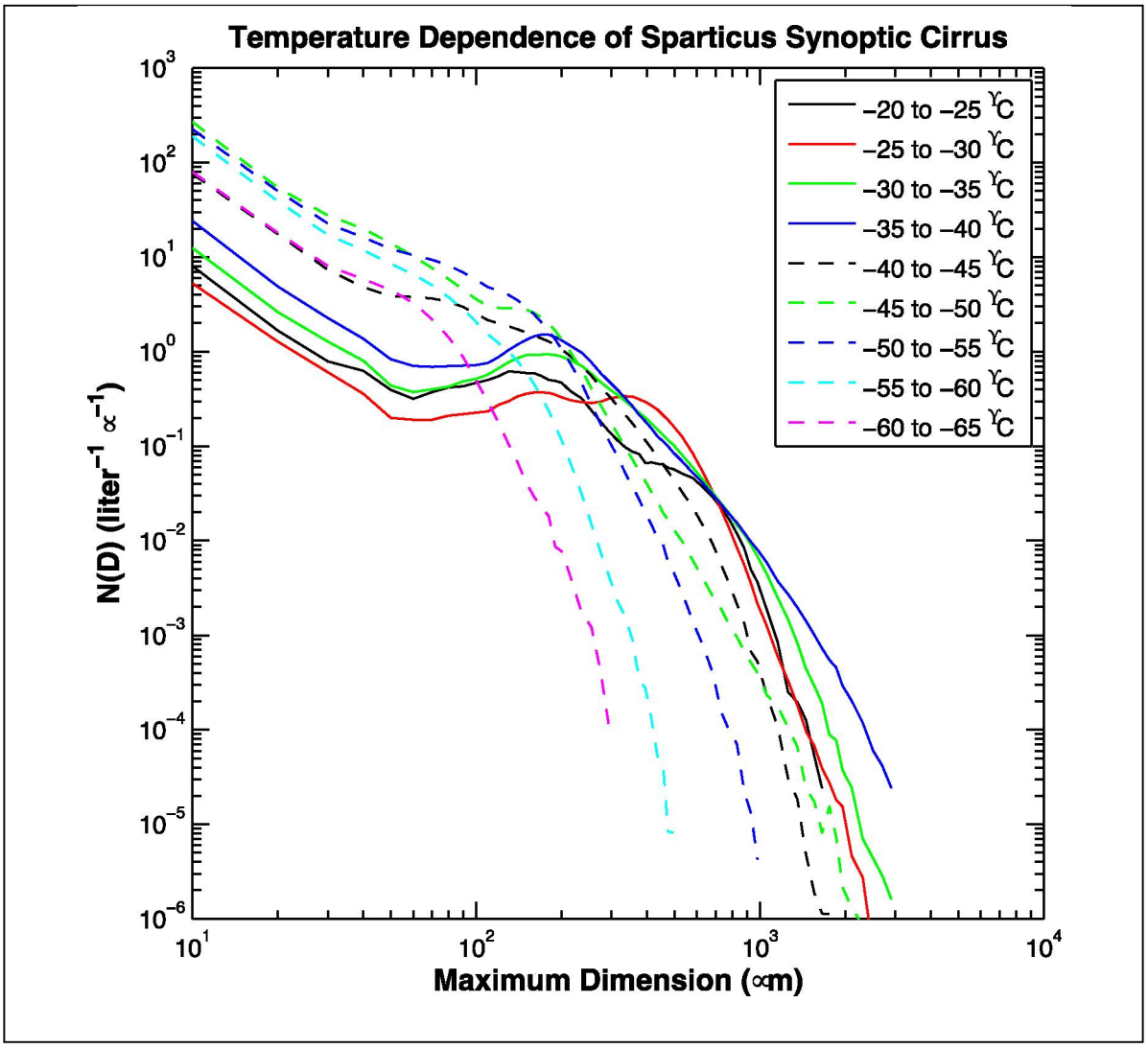

Figure 5. Temperature dependence of ice PSDs in SPartICus synoptic cirrus for temperature ranging from -20 °C to -65 °C. Note that solid lines indicate PSDs for temperatures warmer than the homogeneous nucleation threshold (-40 °C). Dashed lines represent PSDs for temperatures colder than -40 °C.

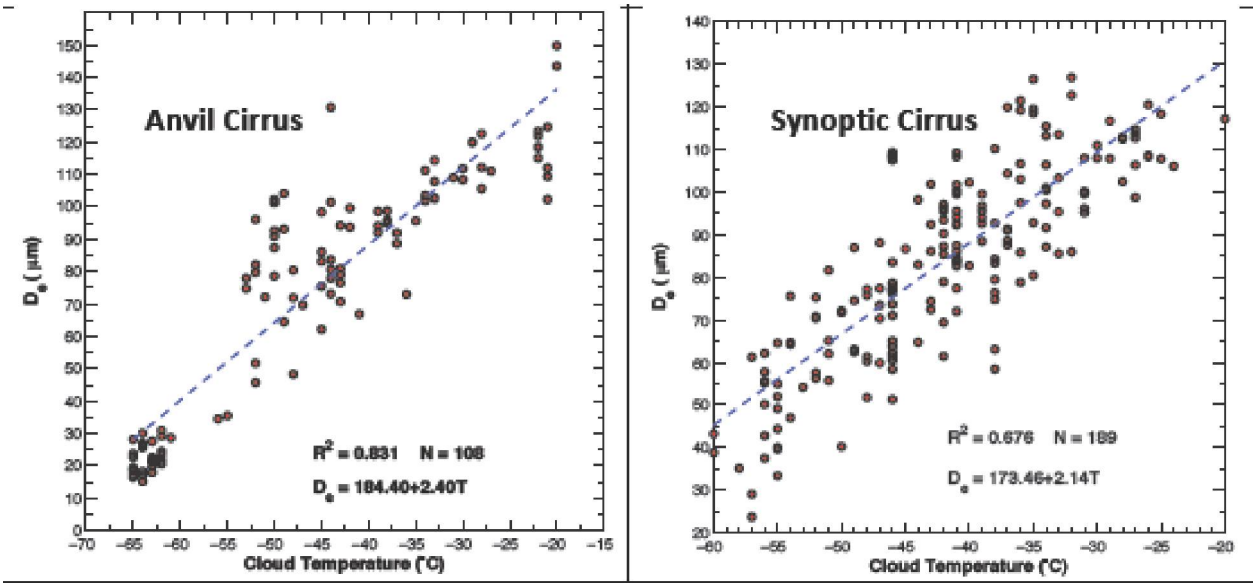

Figure 6. Temperature dependence of D_e for anvil and synoptic cirrus sampled during SPartICus (temperature range -20 ^{o}C to -65 ^{o}C).

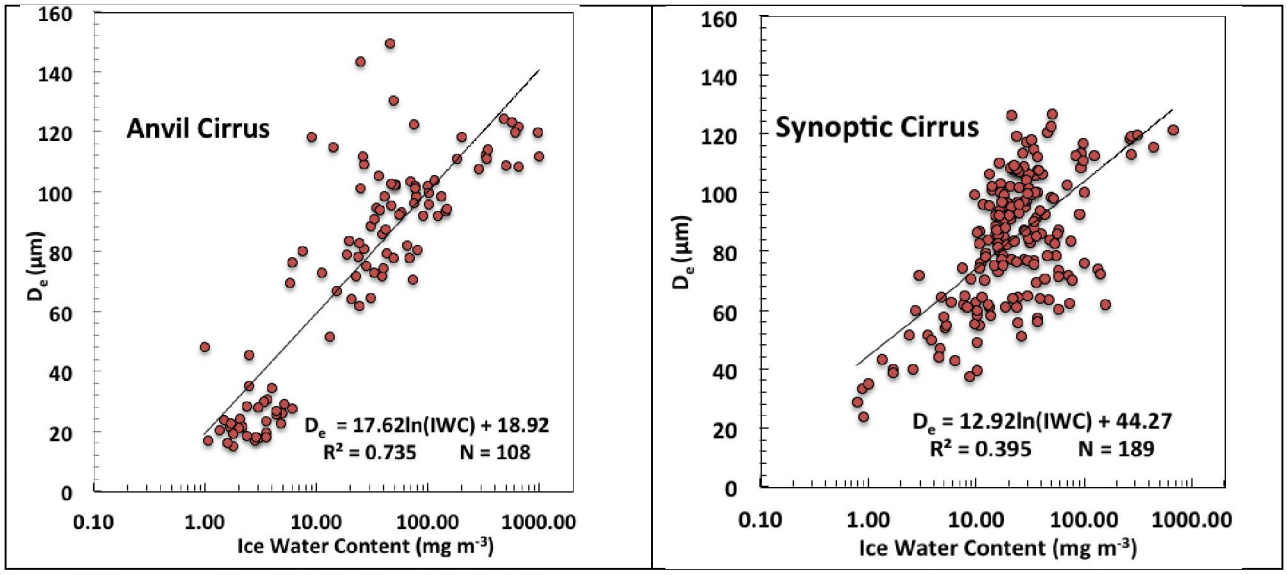

Figure 7. Dependence of D_e on ice water content (IWC) for anvil and synoptic cirrus in SPartICus. N denotes the number of PSDs for the type of cirrus. Temperature range is from -20 °C to -65 °C.

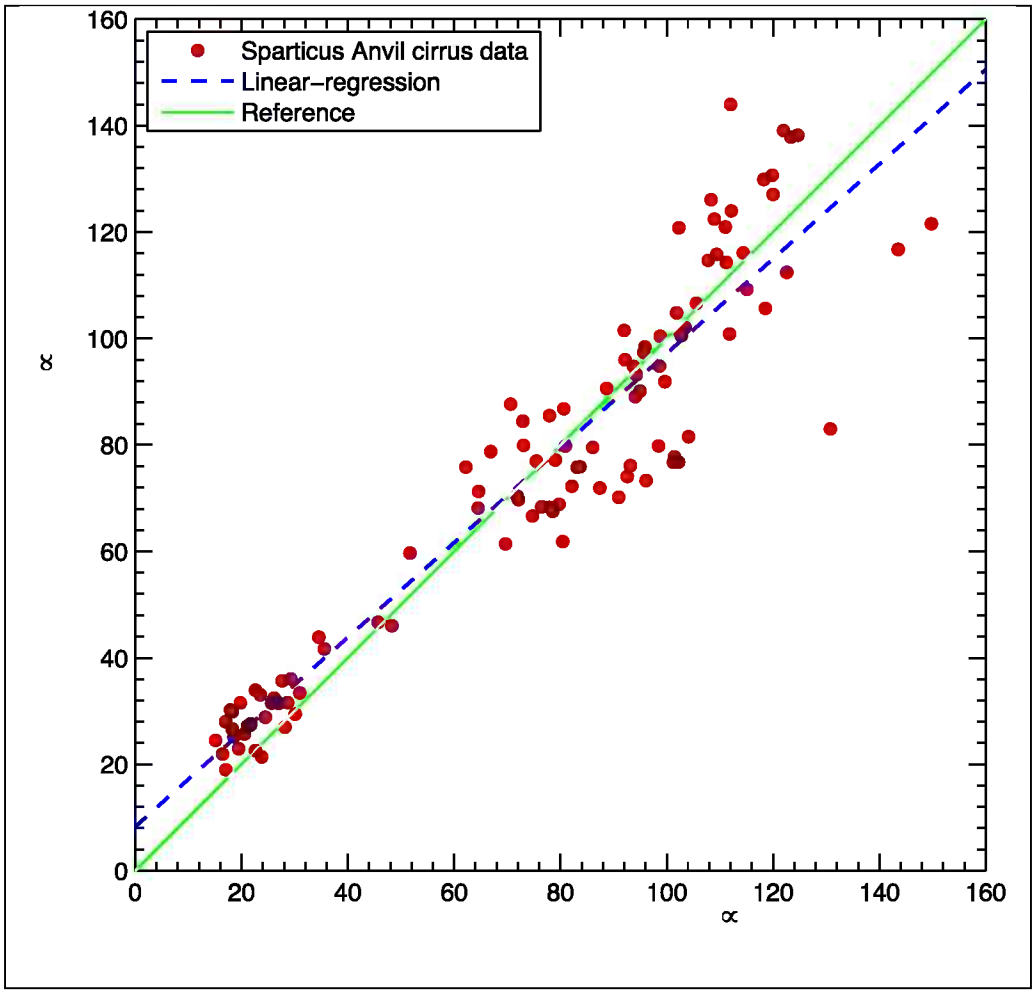

Figure 8(a). Multiple variable regression predicting D_e in terms of temperature and IWC for SPartICus anvil cirrus (temperature range: -20 ^{o}C to -65 ^{o}C).

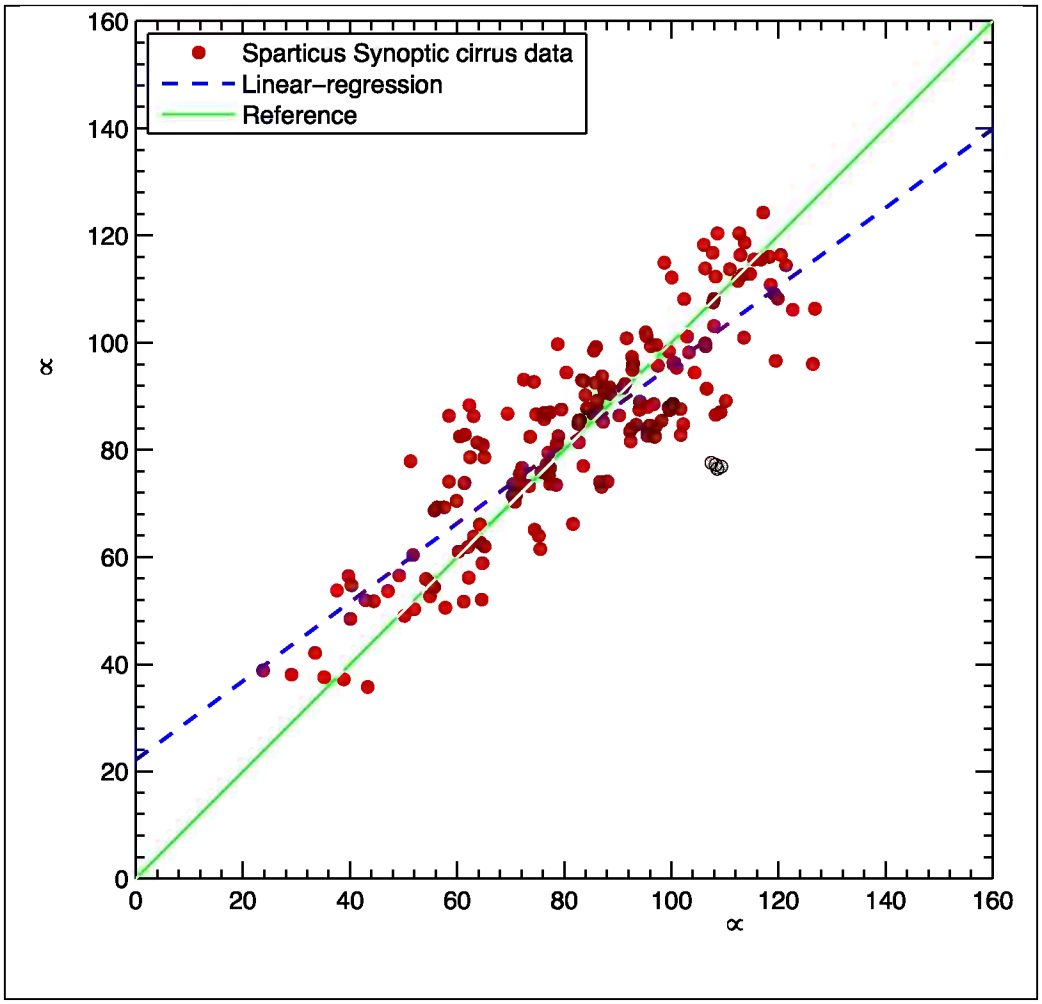

Figure 8(b). Multiple variable regression predicting D_e in terms of temperature and IWC for SPartICus synoptic cirrus data (temperature range: -20 °C to -65 °C).

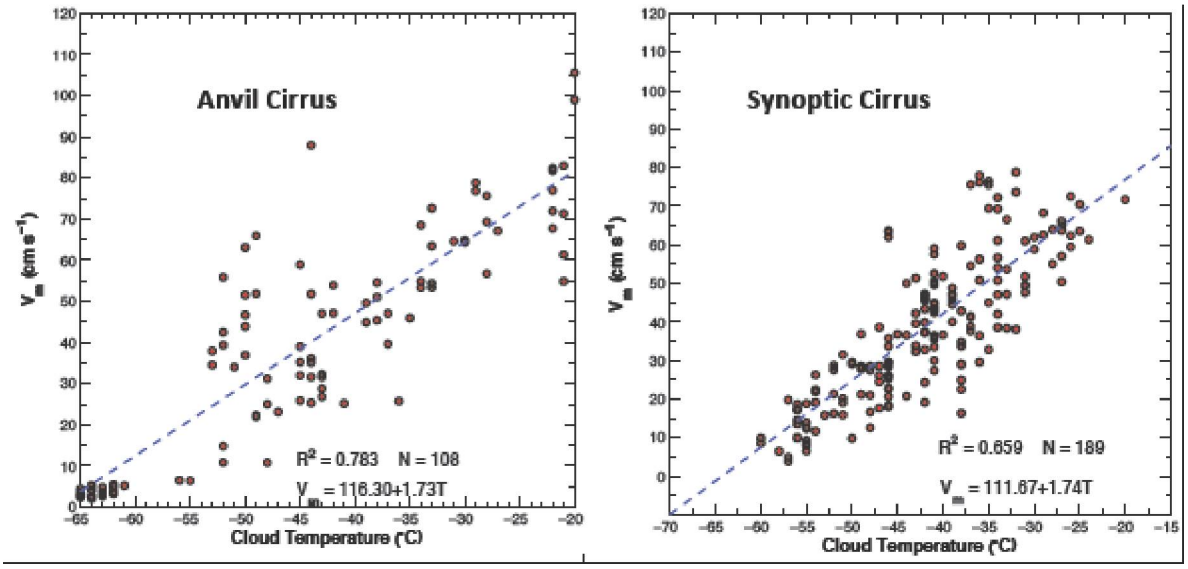

Figure 9. Temperature dependence of V_m for anvil and synoptic cirrus clouds. N denotes the number of PSDs for each type of cirrus (temperature range: -20 °C to -65 °C).

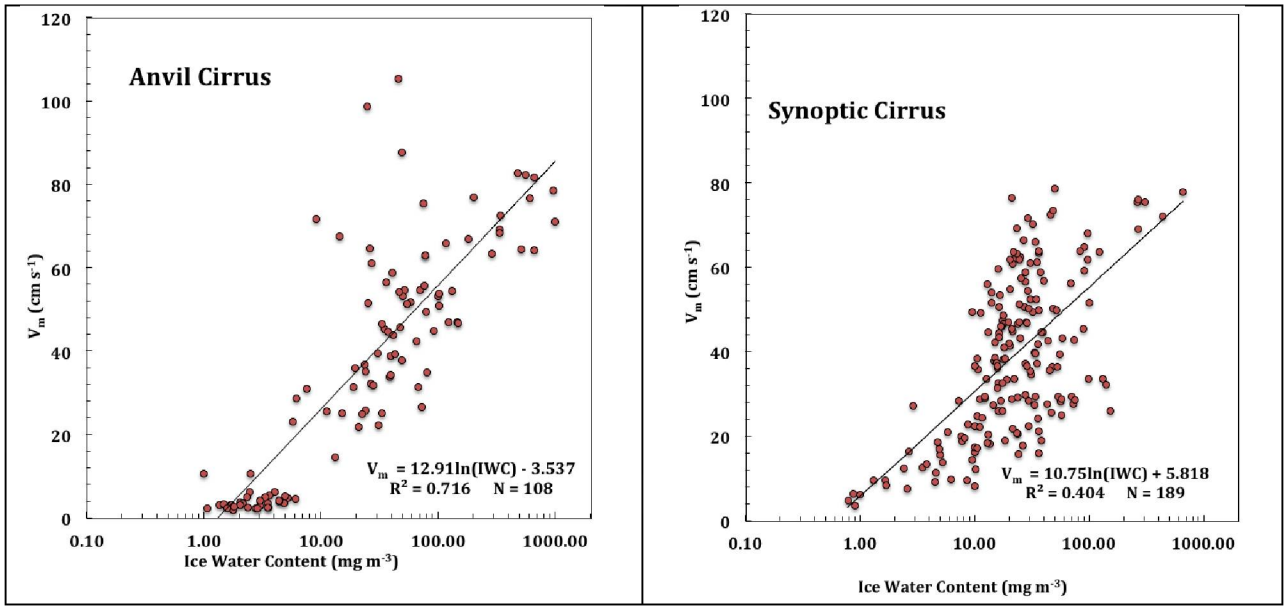

Figure 10. Dependence of V_m on ice water content (IWC) for anvil and synoptic cirrus during SPartICus (temperature range: -20 °C to -65 °C).

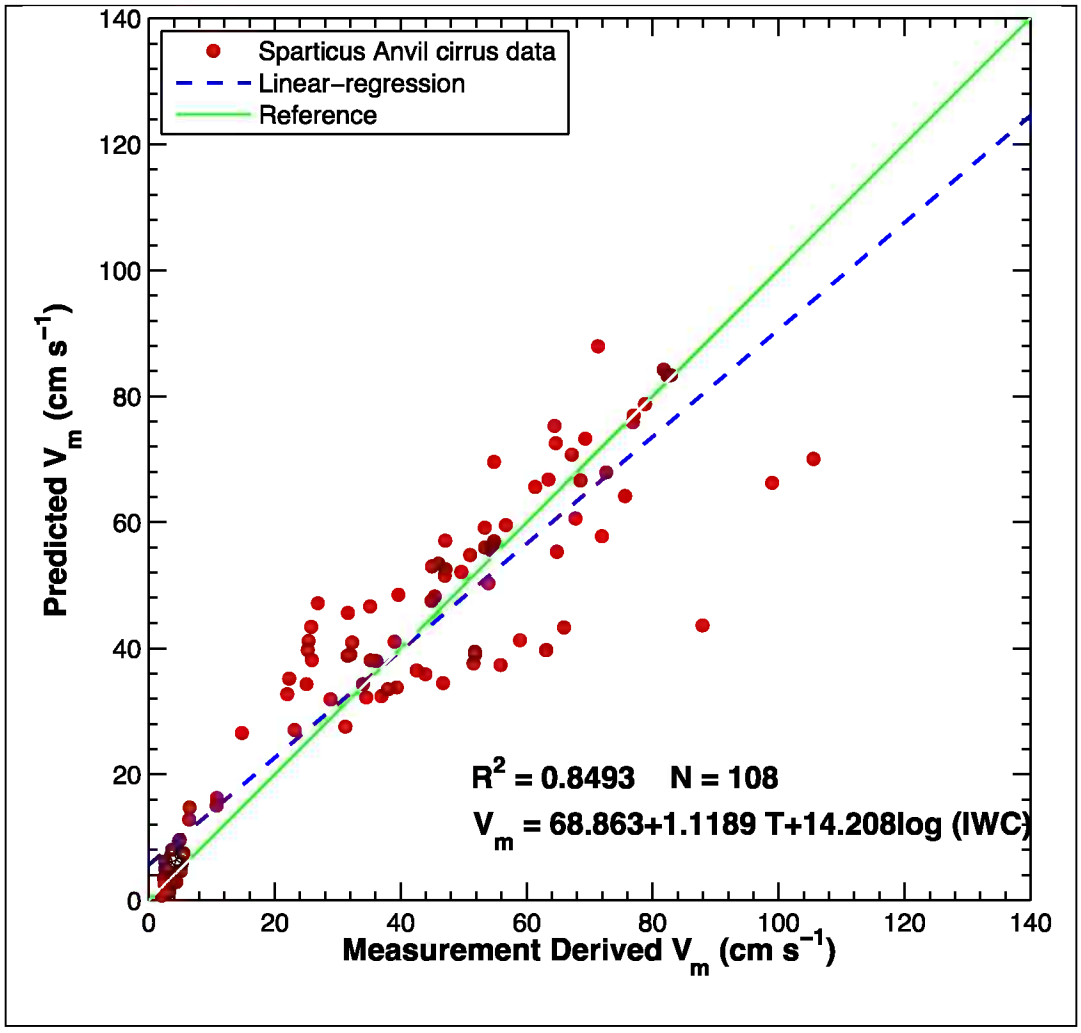

Figure 11(a). Multiple variable regression to predict V_m in terms of temperature and IWC for SPartICus anvil cirrus (temperature range: -20 °C to -65 °C).

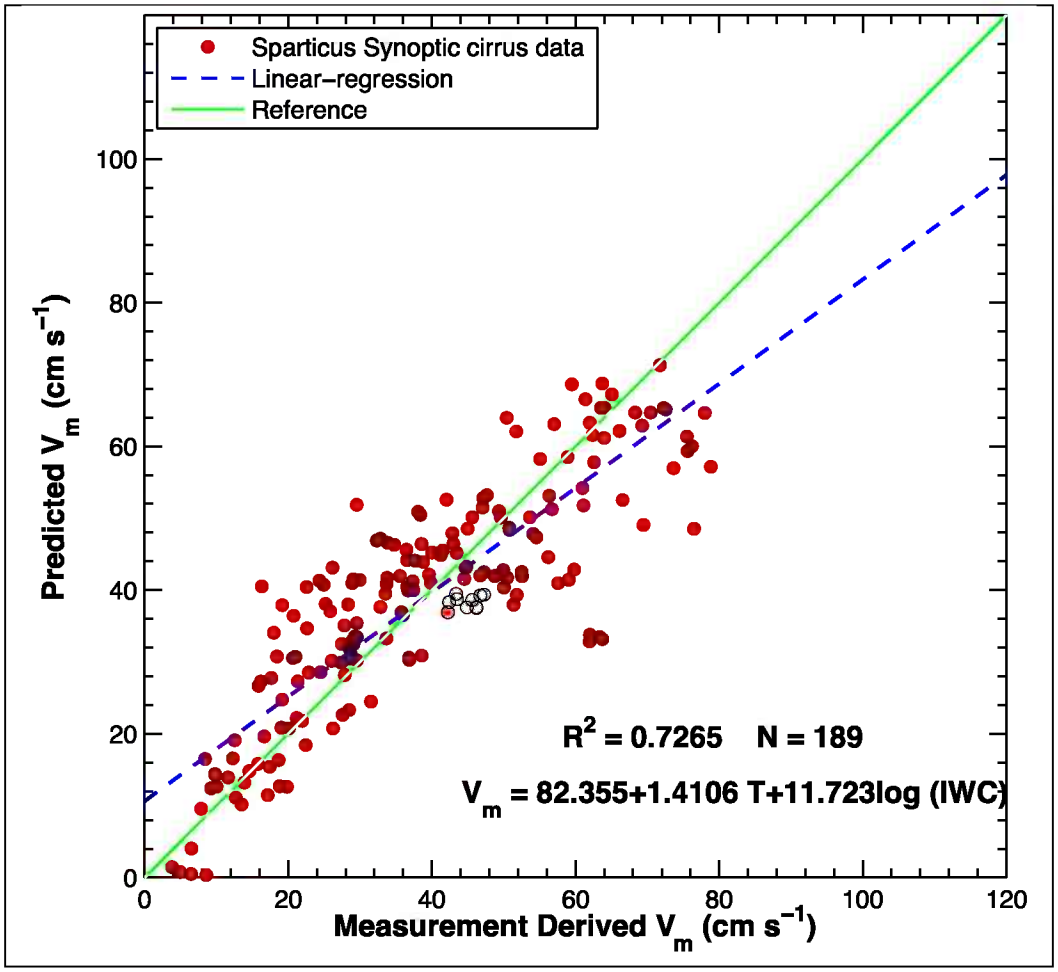

Figure 11(b). Multiple variable regression to predict V_m in terms of temperature and IWC for SPartICus synoptic cirrus. Temperature range: -20 °C to -65 °C.

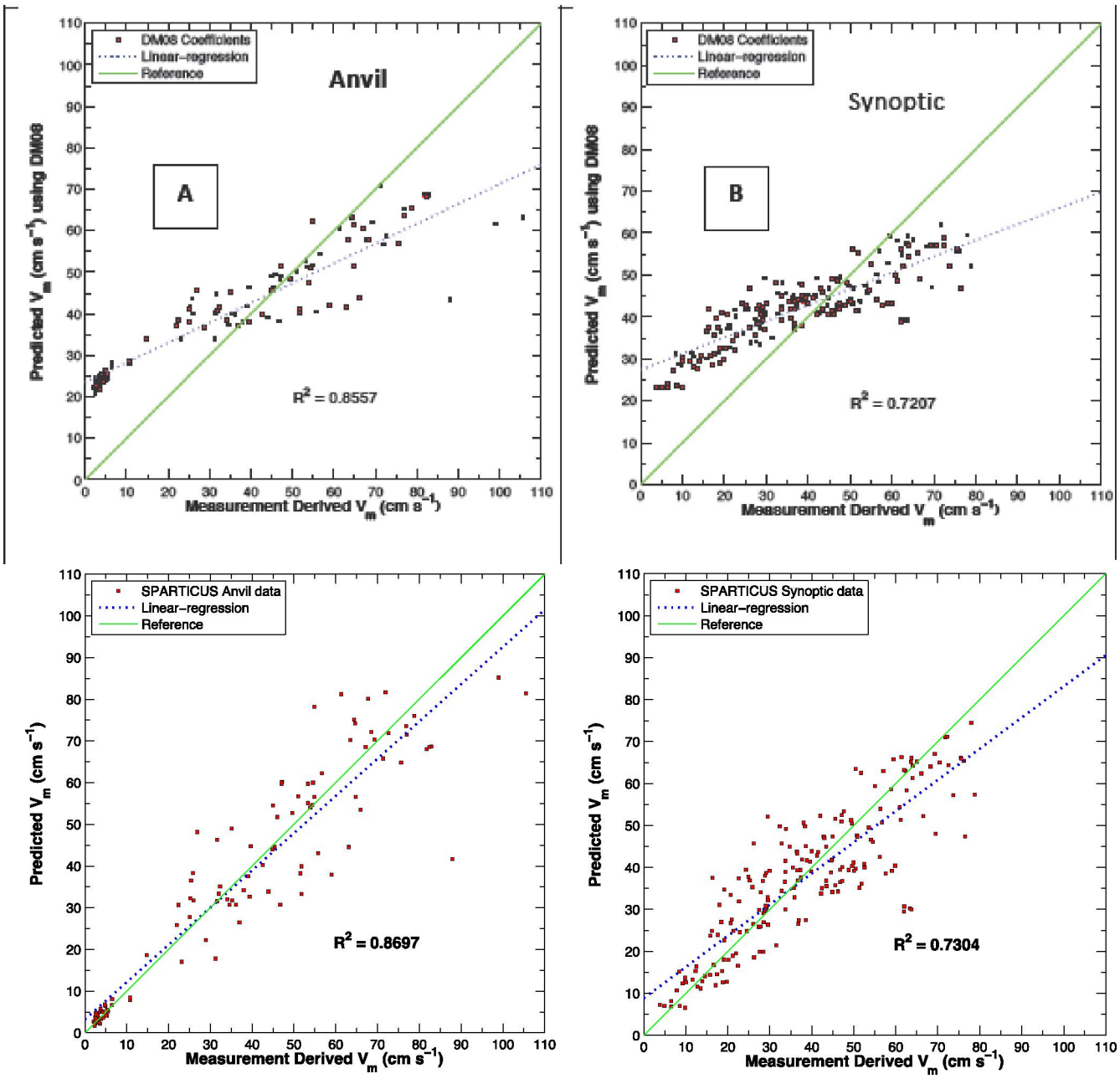

Figure 12. Predicting V_m in terms of temperature and IWC using the formulation of Deng and Mace 2008 (Eq. 10) for SPartICus anvil and synoptic cirrus. A and B are produced by using coefficients derived for SGP cirrus by Deng and Mace 2008. C and D are produced by using coefficients derived from SPartICus data and using the relationship of V_m to T and IWC, as derived by Deng and Mace 2008 (Eqn. 10).

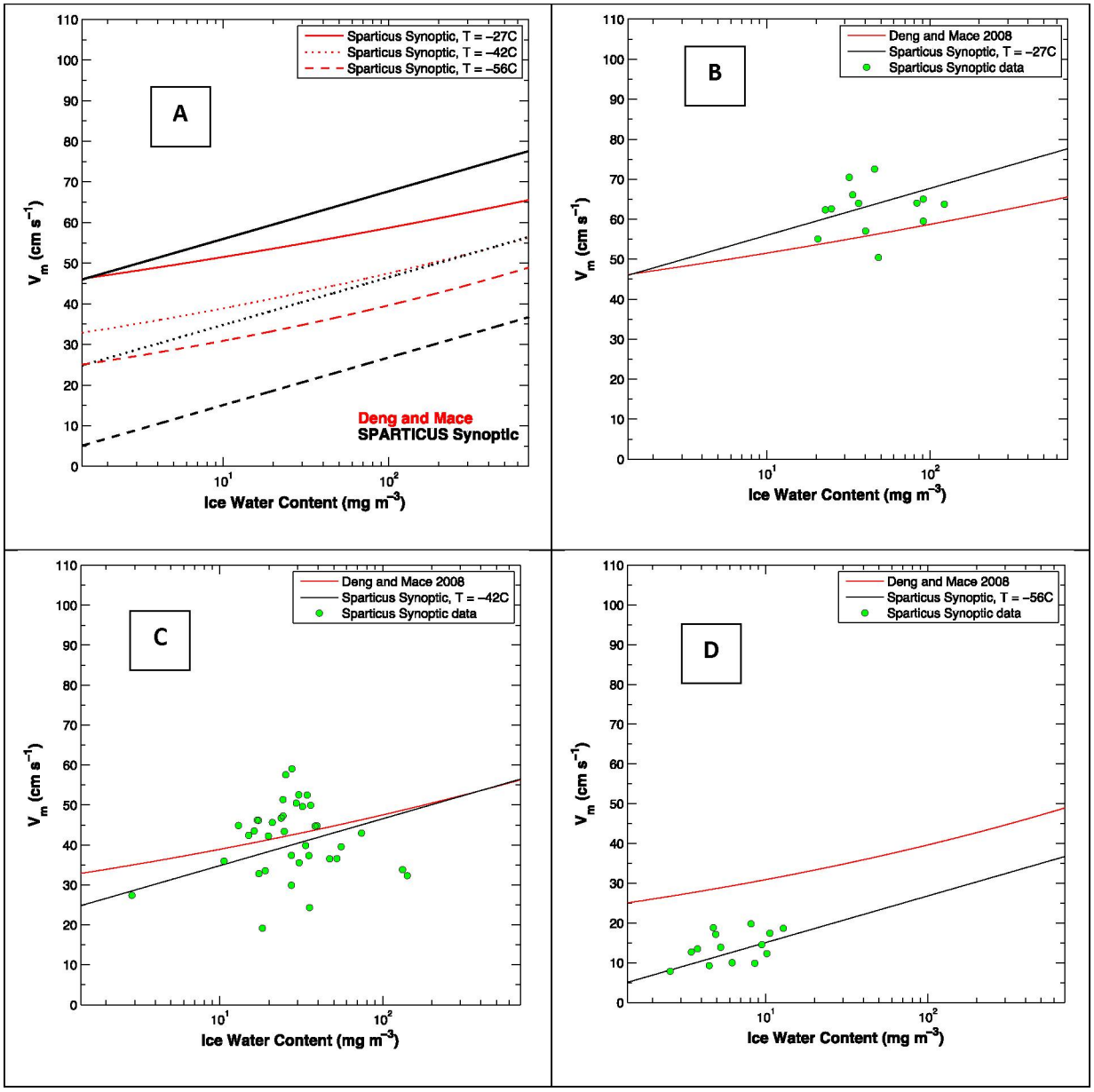

Figure 13. Prediction of mass-weighted fall-speed (V_m) in terms of cloud temperature and IWC, based on Eq. 9 (black curves) and the V_m scheme of Deng and Mace (red curves; Eq. 10) spanning the approximate temperature range of synoptic cirrus sampled in SPartICus. (b) Same but for T = -27°C, comparing measurement derived V_m from -25°C to -28°C; (c) same but for T = -42°C, comparing V_m from -41°C to -43°C; (d) same but for T = -56°C, comparing V_m from -55°C to -57°C.

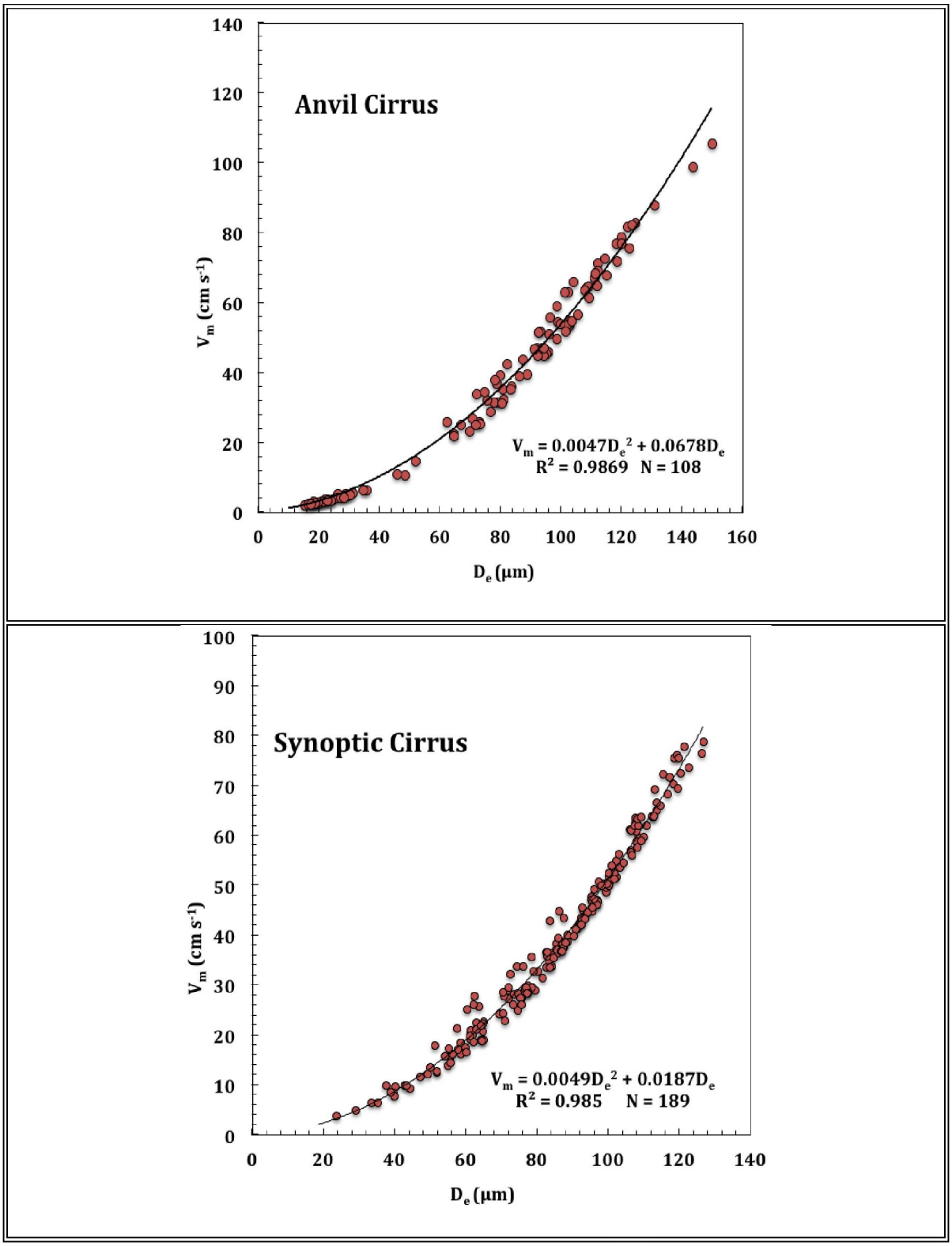

Figure 14. Predicting V_m from D_e for SPartICus anvil cirrus (top) and synoptic cirrus (bottom) using the HW10 formulation. Note that in both the figures, $R^2 > 0.98$.

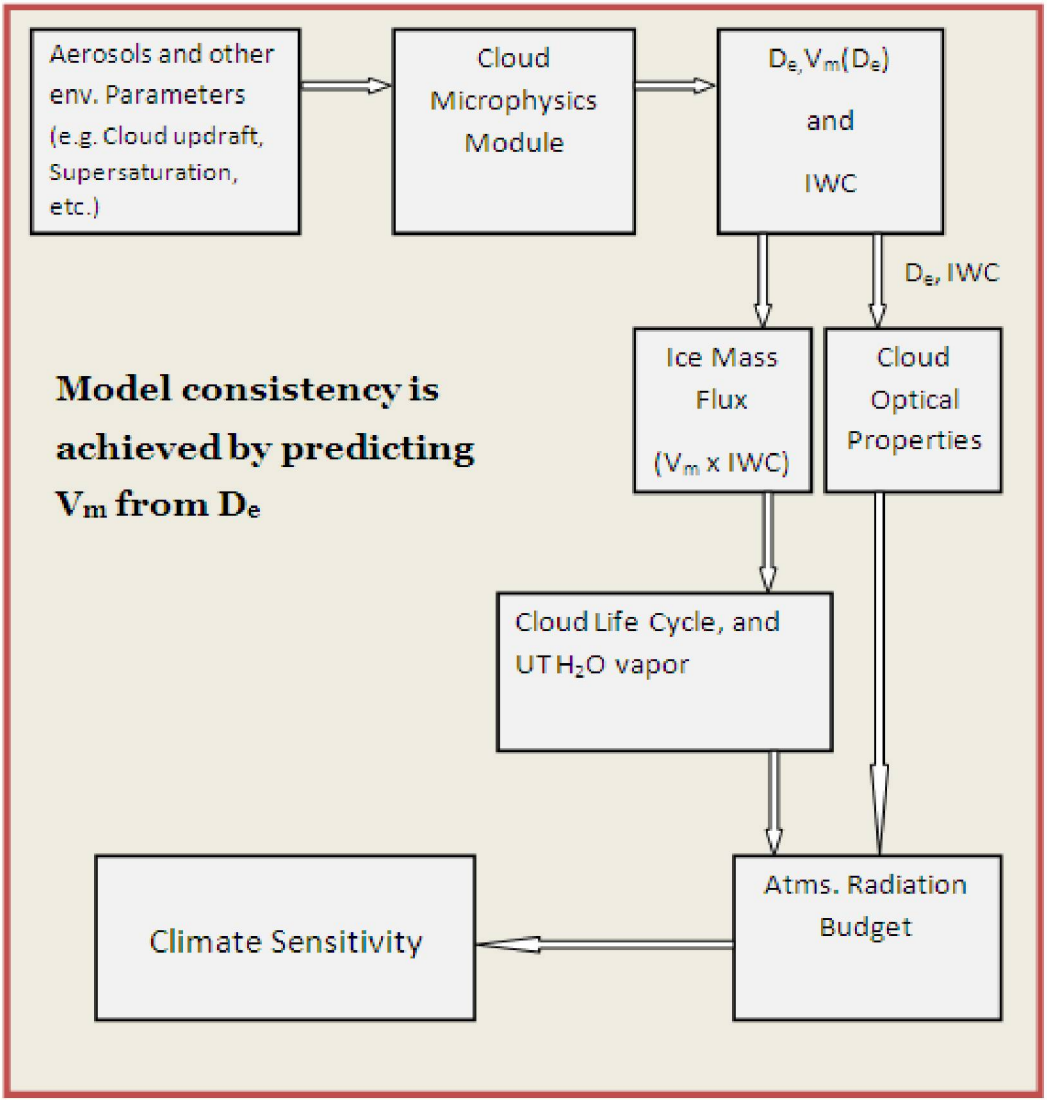

Figure 15. Model consistency diagram suggesting the best way to parameterize V_m to improve the prediction of climate sensitivity. V_m is expressed in terms of D_e, provided that D_e is predicted by the microphysics module and then passed on to the radiation component of the model.